Supporting Information

SI Appendix

Chemicals and reagents

Standard chemicals were purchased from Sigma-Aldrich, Wako, or Nacalai Tesque. Oligos were purchased from Sigma-Genosys, Invitrogen, or Nihon Gene Research Laboratories (NGRL).

Construction of heterodimers carrying single enzyme tags

To define the number of motors, each dimeric motor has to carry a single enzyme tag. Otherwise, the dimeric enzyme tags have a chance to bridge two binding sites on the DNA scaffold. We therefore coexpressed two kinesin polypeptides that form a heterodimer carrying a single enzyme tag in *E.coli*; one polypeptide has an enzyme tag and six-histidine tag, and the other has a FLAG tag. To construct the heterodimer of kinesin-1, the C-terminal truncated kinesin-1 (amino acid residues 1–430, Fig. S1A) from *Rattus norvegicus* was first inserted into a pET-32 (Novagen) derivative vector containing a C-terminal SNAP-tag (snap26b, New England Biolabs) or HaloTag7 (Promega), followed by a six-histidine tag. In the resultant constructs, SNAP-tag/HaloTag7 is C-terminal to the kinesin-1 motor domain (Fig. S1C). The same kinesin-1 fragment was next inserted into another pET-32 derivative vector containing a C-terminal FLAG tag. The resultant expression cassette containing T7 promoter, kinesin-1, FLAG tag and T7 terminator was then inserted into the former vector in tandem with the existing expression cassette containing SNAP-tag/HaloTag7 and six-histidine tag. The linker amino acid sequence between SNAP-tag and kinesin-1 is ELEFP, and between HaloTag7 and kinesin-1 is EL. In the kinesin-1 construct used in this study, cysteine 7 was mutated into serine. This mutation did not affect its motility as reported (1). For an Ncd heterodimer, the N-terminal truncated Ncd (amino acid residues 222–700, Fig. S1B) from *Drosophila melanogaster* was inserted into a pET-32 derivative vector containing an N-terminal six-histidine tag followed by a SNAP-tag. In the resultant construct, SNAP-tag is N-terminal to the Ncd motor domain (Fig. S1D). The same Ncd fragment was inserted into another pET-32 derivative vector containing an N-terminal FLAG tag to construct a heterodimer in the same manner as kinesin-1. The linker amino acid

sequence between SNAP-tag and Ncd is GSEL.

Expression and purification of heterodimer proteins

The kinesin-1 and Ncd constructs were expressed in *Escherichia coli* Rosetta2 (DE3) (Novagen) and BL21 (DE3) Star (Novagen), respectively. The protein expression was induced by 0.1 mM isopropyl β-D-thiogalactoside (IPTG) for 5 h at 20°C. Cells were collected and resuspended in 20 mM Na-Pi buffer (pH7.5) containing 1 mM $MgSO_4$, 250 mM NaCl, 0.1 mM ATP, 1 mM dithiothreitol (DTT), and 10 mM imidazole in the presence of a protease inhibitor cocktail (03969-21, Nacalai Tesque). The resuspended cells were then lysed with a sonicator (Sonifier 250, Branson) and centrifuged to collect the supernatant. From the three types of dimers in the cell lysate, the desired heterodimer was sequentially purified by two different tags. The soluble protein in the supernatant was first bound to a Ni-IMAC resin (156-0133, Bio-rad) and eluted with 20 mM Na-Pi buffer (pH7.5) containing 1 mM $MgSO_4$, 250 mM NaCl, 0.1 mM ATP, 0.5 mM DTT, and 250 mM imidazole. The peak fractions were next bound to an anti-FLAG agarose column (A2220, Sigma-Aldrich) and eluted with 20 mM Na-Pi buffer (pH7.5) containing 1 mM $MgSO_4$, 250 mM NaCl, 0.1 mM ATP, 1 mM DTT, 10 mM imidazole, and 0.35 mg ml^{-1} 3X FLAG peptide (F4799, Sigma-Aldrich). The eluate was further purified by nucleotide-dependent microtubule (MT)-affinity purification (2). Briefly, the eluate was diluted four times with low salt buffer (12 mM piperazine-*N*,*N*'-bis(2-ethanesulfonic acid) (PIPES)-KOH pH6.8, 2 mM $MgCl_2$, 1 mM EGTA), and mixed with ~1 mg ml^{-1} MTs in the presence of 10 μM paclitaxel and 0.5 mM AMP-PNP. The mixed sample was layered on a 10% sucrose cushion and centrifuged at 238,800×g for 15 min at 25°C. The pellet was resuspended with 80 mM K-PIPES buffer (pH 6.8) containing 10 mM $MgSO_4$, 250 mM K-acetate, 10 mM ATP, 1 mM DTT, 10 μM paclitaxel and 10% (w/v) sucrose, followed by centrifugation at 256,500×g for 10 minutes at 25°C. The supernatant was flash frozen in liquid nitrogen and stored at –80°C. Proteins were separated by SDS-PAGE on a 10% polyacrylamide gel that was subsequently stained with Coomassie Brilliant Blue G-250-based reagent (24590, Thermo Scientific). Protein concentration was determined by the Bradford assay using bovine serum albumin as a standard (3).

Design and preparation of DNA scaffold

The nucleotide sequence used as a scaffold was computer-optimized by custom software to minimize undesired structures. The UNAFold algorithm was incorporated into the program to compute a minimum energy folding of the sequence (4). The DNA sequence for the assemblies that engage one to four molecules is:

5’-TTCTTGGCCGAACTGAAGTGATCCAGCTTATAGATATGGGCACGTAAACAAGCATCCGTTGG TCTAGGAGTAGTTACAATTCCCCGGTTCCGCTCATTTCGATTGACCCCTGCGCGTATCATGCTGC ACCACATTAGCCTTCTGTCGTCCCTCTCGCCGCAAAATAGGTACAGTCCTCAGGTGTCTTAAC-3’ (190 nt).

The four thymine bases were used for internal amino modification (Amino-Modifier C6 dT, Glen Research) to anchor the motor proteins (shown in underlined letters). See Fig. S3 for short linker constructs. The above sequence was split into four fragments for oligonucleotide synthesis.

S1F-Cy5, 5’-[Cy5]TTCTTGGCCGAACTGAAGTGATCCAGCTTATAGATATGGGCACGTAA-3’,

S2F, 5’-[P]ACAAGCATCCGTTGGTCTAGGAGTAGTTACAATTCCCCGGTTCCGCTC-3’,

S3F, 5’-[P]ATTTCGATTGACCCCTGCGCGTATCATGCTGCACCACATTAGCCTTCT-3’,

S4F, 5’-[P]GTCGTCCCTCTCGCCGCAAAATAGGTACAGTCCTCAGGTGTCTTAAC-3’.

A letter “P” denotes a 5’-phosphate group that was introduced either by T4 kinase or chemical phosphorylation. To construct a DNA scaffold for the desired motor composition, each DNA fragment was left unmodified or separately modified with a ligand of the desired enzyme tag via amino-reactive *N*-hydroxysuccinimide (NHS) esters. The reaction was performed by mixing the NHS-functionalized ligand (BG-GLA-NHS, New England Biolabs; HaloTag Succinimidyl Ester (O4) Ligand, Promega) and an internally amino-modified DNA strand at 37°C. This reaction keeps the 5’ and 3’ ends of the strand free so that the DNA fragment can be ligated with the other fragments. To join the four fragments into a single DNA scaffold, we used a splint ligation technique using short complementary DNA strands:

S12splint, 5’-ATGCTTGTTTACGTGC-3’,

S23splint, 5’-ATCGAAATGAGCGGAA-3’,

S34splint, 5’-GGGACGACAGAAGGCT-3’.

After overnight ligation, incomplete products and the splint DNA was removed by PAGE purification on a 6% acrylamide/7 M urea gel using homebuilt LED illumination apparatus (Fig. S1F). The electroeluted

DNA scaffold was stored at –80°C. For the DNA scaffold used in a tug-of-war experiment between single kinesin-1 and four Ncds, an additional strand **S5F**, 5’-[P]ATCTCACACTGCTTTAGAGTATGCCTCGGG TTTTATTCTTTGATGAACGCCATTAACCTT-3’ (the underlined letter was amino modified), was joined to the 3’ end of the above mentioned scaffold. An additional splint DNA **S45splint**, 5’-CAGAATTGTAGA GTGT-3’ was used accordingly.

For the control experiment of optical trapping assay, the following oligomeric DNA was used instead of the DNA scaffold described above (Fig. S15):

SBio2_55nt, 5’-[biotin]TTCTTGGCCGAACTGAAGTGATCCAGCTTATAGATATGGGCACGTAAAC AAGCAT[biotin]-3’.

Construction of motor–DNA assemblies

Before conjugation with motor proteins, the DNA scaffold was annealed with the complementary strands shown below (see also Fig. S3).

[Flexible (partial dsDNA)]

S1R, 5’-CTTGTTTACGTGCCCATATCTATAAGCTGGATCACTTCAGT-3’,

S2R, 5’-CGCAGGGGTCAATCGAAATGAGCGGAACCGGGGAATTGTAA-3’,

S3R, 5’-GGACTGTACCTATTTTGCGGCGAGAGGGACGACAGAAGGCT-3’.

[Semi-flexible (nicked dsDNA)]

S1Rfull, 5’-ACCAACGGATGCTTGTTTACGTGCCCATATCTATAAGCTGGATCACTTCAGTTCGGC CAAGAA-3’,

S2Rfull, 5’-AGCATGATACGCGCAGGGGTCAATCGAAATGAGCGGAACCGGGGAATTGTAACTA CTCCTAG-3’,

S3Rfull, 5’-AAGACACCTGAGGACTGTACCTATTTTGCGGCGAGAGGGACGACAGAAGGCTAAT GTGGTGC-3’.

[Rigid (complete dsDNA)]

SRfull, 5’-AAGACACCTGAGGACTGTACCTATTTTGCGGCGAGAGGGACGACAGAAGGCTAA TGTGGTGCAGCATGATACGCGCAGGGGTCAATCGAAATGAGCGGAACCGGGGAATTGTAACTA CTCCTAGACCAACGGATGCTTGTTTACGTGCCCATATCTATAAGCTGGATCACTTCAGTTCGGC

CAAGAA-3’ (187 nt).

For complete dsDNA, the long DNA was prepared by the splint ligation technique from three DNA strands used for nicked dsDNA in the same manner as the above DNA scaffold. The splint DNA sequences are below:

SRfull_splint1, 5’-CCGTTGGTCTAGGAGT-3’,

SRfull_splint2, 5’-ATCATGCTGCACCACA-3’.

Annealing was performed by cooling from 80°C to 25°C at a rate of –2°C per minute with a slight excess of the complementary strands. For optical trapping assays, the complementary strands with dual DIG at both ends were used (Fig. S4):

SDIG2_55ntR, 5'-[DIG]ATGCTTGTTTACGTGCCCATATCTATAAGCTGGATCACTTCAGTTCGGCC AAGAA[DIG]-3'.

Duplex formation was confirmed by PAGE analysis. The motor–DNA assembly was prepared by mixing the DNA scaffold with motor proteins at a molar ratio of 1:3 to 1:5 (calculated per ligand) at 27°C for 1 h. Note that even in the assemblies composed of complete dsDNA, the linkers between DNA and motors include multiple bonds that allow free rotation of the dimer.

Unfortunately, in our hands, the reaction of HaloTag ligand cannot be completed even by a large excess of HaloTag enzyme, unlike the case of SNAP-tag. This caused the problem that the final products for tug-of-war experiments included a considerable amount of assemblies without kinesin-1 as shown by SDS-PAGE (Fig. S20). One complication is that when a fluorescent spot monotonically moves to the MT minus end, we cannot classify it as the consequence of actual tug-of-war, or the movement by assemblies without kinesin-1. We therefore analyzed only the trace that includes plus end-directed movement for more than 300 nm, which ensures that the analyzed runs were driven by both kinesin-1 and Ncd. However, this may lead to overestimation of the average velocity and run length toward the MT plus end.

Removal of an excess amount of free motors

The removal of free motors was performed by using DNA-conjugated magnetic beads (M-280 Streptavidin, Invitrogen; Fig. S5). Briefly, a biotinylated complementary strand of DNA scaffold was first attached to the streptavidin-coupled magnetic beads, and then the DNA scaffolds with motor proteins

containing casein were mixed with the DNA–beads, resulting in duplex formation on the magnetic beads. After extensive washing of the excess amount of free motors in the solution, DNA scaffolds engaging motors were eluted with a complementary strand of the DNA scaffold which is longer than the aforementioned biotinylated complementary strand. The sequence of the biotinylated complementary strand of DNA scaffold is **S1_bind**, 5'-[biotin]AACGTGCCCATATCTATAAGTCGTGCCCATATCTATAAG-3' (the annealing sites were shown in underlined letters), and the complementary strand for elution is **S1R_2**, 5'-CAACGGATGCTTGTTTACGTGCCCATATCTATAAGCTGGATCACTTCAGTTCGGCCAAG-3'.

Preparation of tubulin and MTs

Tubulin was purified from porcine brain by two cycles of assembly/disassembly and chromatography on a phosphocellulose column (P11, Whatman) (5). The Cy3 and biotin labeling of tubulin was performed as described (6). Cy3-biotin-MTs were polymerized by copolymerizing Cy3-biotin-tubulin (labeling stoichiometry of 4% for Cy3) and unlabeled tubulin at a ratio of 1:5 for 30 min at 37°C, and stabilized with 40 μM paclitaxel (T1912, Sigma-Aldrich). Polarity-marked MTs were polymerized from brightly fluorescent, fragmented Cy3-axonemes from *Chlamydomonas reinhardtii* in the presence of a 2.3 : 3.7 : 1 ratio of NEM (*N*-ethylmaleimide)-treated, NEM-untreated, and Cy3-tubulin (19% labeling stoichiometry) for 20 min at 37°C, and then stabilized with 40 μM paclitaxel.

Imaging for single fluorescence tracking assays

Single fluorescence tracking assays were performed using a homebuilt, objective-type total internal reflection fluorescence microscope (IX70, Olympus) equipped with a 60×/NA1.45 oil immersion objective lens (PlanApo, Olympus). Images were magnified by 3.3×TV-adaptor, split into two side-by-side images of Cy3 and Cy5 using a DualView system (Optical Insights), and projected onto a back-illuminated EMCCD detector (C9100-13, Hamamatsu Photonics). The exposure time and frame rate was 70 ms per frame. Cy3 and Cy5 were excited using a diode-pumped solid-state laser (532 nm; CDPS532S-020, JDS Uniphase) and a He-Ne laser (632.8 nm; 30991, Research Electro-Optics), respectively. The position of the Cy5 dye was determined by a custom automated tracking program

(MARK 2.5) using a two-dimensional Gaussian fitting algorithm (7) after four-frame rolling averaging. The program stops tracking when it misses the Cy5 spot for more than four frames. The standard deviation of the position of Cy5 spots rigidly bound on a glass surface was about 16 nm.

Single fluorescence tracking assays

The movement of individual Cy5 dyes was observed at 24 ± 1°C essentially as described (8). A flow chamber was constructed using two coverslips (18×18 mm and 24×32 mm, thickness No.1; Matsunami Glass) and 80 μm thick double-sided sticky tape (W-12, Scotch 3M) to create a chamber that was 3 mm wide and 18 mm long. The 24×32-mm coverslips were cleaned and silanized as described (9) with the following modifications. The uncoated coverslips were cleaned by 2% Hellmanex II (Hellma) in Milli-Q water for 20 min with heat (2510, Branson) instead of 0.1 M KOH. Before silanization, the surface was activated with oxygen plasma for 1 min (PDC-32G, Harrick). To immobilize MTs, the flow chamber was first coated with 20 μg ml^{-1} Neutravidin (31000, Thermo scientific) in BRB80 buffer (80 mM PIPES-KOH pH 6.8, 2 mM $MgCl_2$ and 1 mM EGTA), allowed to adsorb for 5 min, and blocked with 1% (w/v) Pluronic F-127 (P2443, Sigma-Aldrich) in BRB80 buffer. After washing with 0.6–0.7 mg ml^{-1} casein (07319-82, Nacalai Tesque) in BRB80 buffer, the flow chamber was incubated with Cy3-biotin-MTs solution in BRB80 buffer for 5 min. After washing with casein solution, the chamber was filled with imaging solution containing 100–500 pM DNA–motor assemblies, 12 mM PIPES-KOH pH 6.8, 2 mM $MgCl_2$, 1 mM EGTA, 15 mM K-acetate, 10 μM paclitaxel, 0.6–0.7 mg ml^{-1} casein, 2 mM DTT, 25 mM glucose, 42.5 U ml^{-1} glucose oxydase (G-2133, Sigma-Aldrich), 1,600 U ml^{-1} catalase (531-73831, Calbiochem), and 1 mM ATP. In this condition, MT gliding was not observed. After the data were recorded, the polarity of MTs was determined by observing the direction of the movement of Alexa647-labeled kinesin-1 molecules. Run length is defined as the distance between the appearance and disappearance of a Cy5 spot on a MT. Runs that moved for more than 200 nm and two frames were analyzed. The motors that reached the edge of the microscope field of view or the microtubule ends were treated as detached. Velocity of each run was determined by linear fitting. The average velocities and run lengths were determined as follows: for each independent experiment, the mean value was calculated from the arithmetic mean of the raw data. These values from three to four independent experiments were then

averaged to determine the representing average value for each construct. For each independent experiment, we used protein samples from different preparation batches but used DNA scaffolds from the same preparation. The averaged run lengths were corrected for the photobleaching rate (0.0070 s^{-1}) as previously described (10). Fluorescence intensity and photobleaching behavior were analyzed by integrating intensities from 9×9 pixels and subtracting the background. The mean-squared displacement (MSD) was plotted by averaging squared displacement for nonoverlapping intervals τ (11). The diffusion coefficient and mean drift velocity were determined by fitting MSD with $\mathrm{MSD}(\tau) = 2D\tau + v^2\tau^2 + C$ to the first several time intervals of the obtained MSD plots (τ, time interval; D, diffusion coefficient; v, drift velocity; C, constant).

Instrumentation for optical trapping assays

Optical trapping were performed essentially as described (12, 13). Beads were trapped and positioned over fluorescently labeled MTs or polarity-marked MTs by a focused Nd:YAG laser (1064 nm, Spectra Physics) using a 60×/NA1.45 (IR) oil immersion objective lens (PlanApo, Olympus). The bead was illuminated diagonally by a collimated red laser beam (632.8 nm, Melles Griot). The light scattered by the bead was gathered by the same objective lens and passed through a custom-made perforated mirror (5 mm in diameter when viewed from the optical axis, Sigma Koki) placed below the objective lens (14). The dark-field image of the bead was projected onto a quadrant photodiode (S994-13, Hamamatsu Photonics) coupled to a differential amplifier (OP711A-2, Sentec). The bead position was recorded at a sampling rate of 10 kHz and anti-alias filtered to 5 kHz before digitization by a 16-bit A/D module (USB-6251, National Instruments). Cy3-MTs and dark-field images of the beads (just for manipulation) were simultaneously visualized by total internal reflection fluorescence microscopy using a diode-pumped solid-state laser (532 nm; Excelsior-532-200-CDRH, Spectra Physics). Images were split into two side-by-side images of Cy3-MT and beads using a dichroic mirror, and projected onto a cooled EMCCD detector (Luca, Andor Technology). The exposure time and frame rate was 70 ms per frame. The sample was mounted on a piezo electric stage (P-517.3CD, Physik Instrumente). Linearity between the monitored and actual displacement of the bead from the trap center was verified up to ±200 nm by applying a sinusoidal movement to the

piezo stage and analyze the response of the photodiode sensor. The bead position was calibrated for each bead by moving the photodiode sensor in a stepwise manner (15). The trap stiffness was calculated for each bead from the amplitude of the thermal diffusion using the equipartition theorem. The trap stiffness calculation was frequently cross-checked by using power spectral measurements (Fig. S13). The sample was applied a sinusoidal movement to obtain a calibration peak as previously described (16).

Optical trapping assays

Carboxylate-modified polystyrene beads with a diameter of 0.21 μm (F8811, Invitrogen) or 0.45 μm (09836, Polysciences) were incubated with 0.6 μg of anti-DIG antibody (11333062910, Roche) in 50 μl of BRB80 buffer for 20 min at room temperature. The final concentration of 0.21-μm and 0.45-μm bead was about 650 pM and 64 pM, respectively. The bead surface was then blocked with 1 mg ml^{-1} casein for 10 min, followed by extensive washing with BRB80 buffer using a tabletop centrifuge. The collected beads were resuspended with 50 μl of BRB80 buffer and sonicated for 15 s (VS-25, Velvo-Clear). The resulting DIG-beads were then mixed with motor–DNA assemblies for 15 min at room temperature, followed by washing with BRB80 buffer. To avoid multiple assemblies on a bead, the motor–DNA assembly was mixed with the bead at sufficiently low concentration such that the binding fraction of the beads onto MTs was less than 30%. This ensures that >90% of the beads that moved on a MT were driven by a single-*assembly* (17). Construction of a flow chamber is performed as described in the section “Single fluorescence tracking assays” above. Trapping experiments were performed at 24 ± 1°C. To immobilize MTs, the flow chamber was first coated with 10 μg ml^{-1} anti-β-tubulin antibody (SC-58884, Santa Cruz) in BRB80 buffer, allowed to adsorb for 5 min, and blocked with 1% (w/v) Pluronic F-127 in BRB80 buffer. After washing with 0.6–0.7 mg ml^{-1} casein in BRB80 buffer, the flow chamber was incubated with Cy3-MTs or polarity-marked Cy3-MTs solution in BRB80 buffer for 5 min. After washing with casein solution, the chamber was filled with imaging solution containing motor–DNA–beads, 12 mM PIPES-KOH pH 6.8, 2 mM $MgCl_2$, 1 mM EGTA, 15 mM K-acetate, 10 μM paclitaxel, 0.6–0.7 mg ml^{-1} casein, 2 mM DTT, 25 mM glucose, 21.3 U ml^{-1} glucose oxydase, 800 U ml^{-1} catalase, and 1 mM ATP. The average maximum forces are determined by averaging the force corresponding to the maximum height of each peak. The stall force was determined by averaging the force of plateaus that lasts for more

than 200 ms just prior to detachment. The forces were analyzed manually after low-pass filtered to 25 Hz.

Bead assays in the absence of the trapping force

We tested the possibility that some of the kinesin-1 motors are damaged when adsorbed to a bead surface by measuring the run length of the two-kinesin bead in the absence of the trapping force (Fig. S14). The assemblies containing either single or two coupled kinesin-1 motors (7.0-nm spacing) were attached on the beads via anti-DIG antibody, and then the beads were positioned over MTs with a weak optical trap (~0.01 pN nm^{-1}). When the beads attached to the MT, the trap was immediately turned off, although they can typically escape from the weak trap. The movement in the absence of the trapping force was captured by EMCCD camera and analyzed as described above for Cy5 dyes. The binding fraction of the beads onto the MTs was adjusted to be less than 30% to ensure the single-*assembly* range.

Control experiment for optical trapping

We tested the possibility that one of the linkages in the bead–motor assembly breaks before the motors unbind from MTs. To do this, we observed the unbinding of motorless assemblies attached on a 0.45-μm bead from a NeutrAvidin-coated surface (Fig. S15). As a result, we never observed unbinding of the beads from the surface with a trap stiffness of up to 0.3 pN nm^{-1} at various loading rates using a piezo electric stage. To avoid multiple assemblies on a bead, the binding fraction of the beads onto the NeutrAvidin-coated surface was adjusted to be less than 30%. The binding fraction was determined by counting the bound beads after each trapped bead was positioned onto the NeutrAvidin-coated surface for 3 s. When omitting two biotins or DIGs on DNA, we rarely observed the surface attachment of the beads. This ensures that the beads were bound to the surface via specific linkages, including biotin–avidin, antigen–antibody, and DNA–DNA linkages.

Monte Carlo simulation for multiple kinesin-1 motors

The simulation model is based on the previous studies (18, 19). Each motor is a stochastic stepper that binds to discrete binding sites on the MT track. The MT track is a flat, two-dimensional surface. The binding sites are located every 8 nm for the long axis and 6 nm for the short axis of the track, respectively.

The width of the track is assumed to be 48 nm based on a simple geometric configuration in which kinesin with a 17-nm length does not interfere with a glass surface (Fig. S7A). The length of the track $x_{\max}$ is set to the experimentally measured average length of the MT. The linkage between motors including DNA, the coiled-coil stalk of the motors, enzyme tag, and spacers between them is modeled as a special spring that exerts Hookean restoring force only when stretched beyond its rest length. The rest length of the linkage is estimated by the end-to-end length of the DNA for simplicity. The end-to-end length of DNA can be calculated from the mean-squared end-to-end length

$$\langle R^2 \rangle = 2P^2 \left[\exp\left(-\frac{L}{P}\right) - 1 + \frac{L}{P} \right],$$

where P is the persistence length, and L is the contour length (20). For single stranded DNA, in low ionic strength conditions, P is 3 nm, and L is 0.6 nm per base (21). For double stranded DNA, P is 50 nm, and L is 0.34 nm per base (22). The nonlinear elasticity of the linkage may cause a systematic error in the estimation of linker-length dependence of velocity and run length. To describe the system's behavior more closely, it may be required to build a more realistic model of the linkage based on the experimental measurement.

The outline of the algorithm:

1. Simulation starts with a randomly selected single motor attached to the track at a random position.
2. For each time step, repeat the following procedures for each motor in random order.
   (i) If the motor is currently detached, test attachment and determine its binding site on the track.
   (ii) If the motor is currently attached, calculate the force it feels and test force-dependent detachment and stepping.
3. If the termination condition is satisfied, record the current time and run length, else go to step 2.

The details of the algorithm are as follows. Simulation starts at time $t = 0$ with a randomly selected single motor (ith motor) attached to the track at a random position x_i and y_i on the long and short axis of the track, respectively. For each time step ($\Delta t = 10$ μs), we determine the state (attached or detached) and position of each motor in random order. This means that we update the states and positions

of the motors sequentially but once for each motor for each time step Δt. If the motor of interest is currently detached, then the motor has a chance to attach with a probability $P_{\mathrm{on}} = \pi_0 \times \Delta t$. The on-rate π_0 is assumed to be constant. The attachment site is determined as follows. If the motor to be bound is tethered to the track via a single linker, then we allow it to attach to the binding sites within a circular area of radius L, the end-to-end length of the DNA linker (Fig. S7B). The lower limit for L is set to 8 nm. This means that when the length of the DNA linker is shorter than 8 nm, we allow the motor to attach to the binding sites within a circular area of radius 8 nm. If the motor is tethered to the track via two linkers, then we allow it to attach to the binding sites within the overlapped region of the two circular areas of radius L_1 and L_2, the end-to-end lengths of the two DNA linkers (Fig. S7C). Note that the linker can include detached motors, as shown in Fig. S7C. When the two linkers are stretched beyond their rest lengths, the attachment site is uniquely determined on the line between the two attached motors: the attachment site divides the line according to the ratio of the linker length. If all binding sites within the region are occupied by the other motors, then we leave the motor detached. Since we found that the probability distribution of binding sites within a region is not crucial for the results, the distribution is set to uniform over the region.

If the motor of interest (ith motor) is currently attached, all force vectors $\overrightarrow{\boldsymbol{F}_{i,j}} = \kappa \times \Delta\overrightarrow{\boldsymbol{l}_{i,j}}$ felt by ith motor are calculated, where κ is the linkage stiffness and $\overrightarrow{\Delta\boldsymbol{l}_{i,j}}$ is the extension of the linkage between ith motor and jth motor; jth motor is bound on the track and connected with ith motor via a linker. Detachment probability P_{off} is calculated as

$$\varepsilon_0 \Delta t \times \exp\left(\left\|\sum\nolimits_j \overrightarrow{\boldsymbol{F}_{i,j}}\right\| / F_{\mathrm{d}}\right),$$

where $\|...\|$ denotes the norm of a vector, ε_0 is the detachment rate at no load, and F_{d} is the characteristic force of detachment. If the motor of interest did not detach in the above procedure, stepping probability is calculated depending on the direction of the net force it feels. If the motor feels a forward load, the stepping rate is constant ($k_{\mathrm{step}} = 98.3\ \mathrm{s}^{-1}$) and independent of the load. If the motor feels a backward load smaller than the stall force $F_{\mathrm{s}} = 6.8$ pN, then the stepping rate is given by the equation

$$k_{\mathrm{step},F} = k_{\mathrm{step}}\left[1 - \left\{\left\|\left(\sum\nolimits_j \overrightarrow{\boldsymbol{F}_{i,j}}\right)_x\right\| / F_{\mathrm{s}}\right\}^w\right],$$

where $\left(\sum_j \overrightarrow{\boldsymbol{F}_{i,j}}\right)_x$ is the x component of the force applied to the ith motor, F_{s} is the stall force, and w is a parameter that describes the force–velocity relationship of the motor. For a backward load greater than the stall force, the stepping rate is set to zero. The motor steps forward in 8-nm increments with the probability $P_{\mathrm{step}} = k_{\mathrm{step},F} \times \Delta t$, unless it encounters the other motors. As a read-out for transport, the position of the MT bound motor nearest to the 5' end of the DNA scaffold is recorded. The termination conditions are that (1) all motors are detached, (2) the current time t exceeds 10^8 s, and (3) the position x_i is greater than $x_{\max}$ for all motors. Upon termination, the current time t and run length are recorded. The fixed parameters for kinesin-1 (F_{d} and w) were taken from the previous study (18). The parameters used are listed in Table S6. The uniformly distributed random numbers were drawn using the Mersenne twister algorithm (23).

Monte Carlo simulation for multiple Ncds

The Ncd model has one major difference from the kinesin-1 model. In Ncd model, the thermal agitation drives single Ncd motors bidirectionally along MTs. Prior to the evaluation of active stepping, we tested random stepping. If there is only one motor in the assembly that binds to a MT, the motor has a chance to take a random step. The displacement of each step is drawn from a Gaussian distribution with mean-square displacement $2D\Delta t$, where D is the diffusion coefficient of single Ncd motors. The displacement of a random step is not required to be multiple of 8 nm, i.e., fractional steps are allowed for passive stepping, assuming that these steps are taken in the weakly bound states such as ADP bound states (8). If the displacement of the random step is smaller than the specified threshold ("lower limit of random steps" in Table S6), the motor has a chance to take a unidirectional step instead of the random step. If there are multiple motors bound to a MT, then the motors can avoid the thermal kick and has a chance to take a unidirectional step. Just as kinesin-1 model, the motor actively steps forward in 8-nm increments with the probability $P_{\mathrm{step}} = k_{\mathrm{step},F} \times \Delta t$, unless it encounters the other motors. The values for the fixed parameters including the stall force and force–velocity curve were speculative because little is known about

these parameters for Ncd. However, the scanning of all parameters is not applicable due to the practical problem of calculation time. Instead, we fixed some parameters in the reasonable range and then scanned the other parameters that are assumed to be more influential (Fig. 4C, S16, and S18). Specifically, the value of stall force was chosen as an upper bound based on a previous study (24), and the force–velocity curve was assumed to be linear, which is measured for mitotic Eg5 (25). The simulations for Ncd show that the stall force and force–velocity curve affected the motility only to a limited extent (Fig. S19).

Monte Carlo simulation for optical trapping

The models are identical for kinesin-1 and Ncd for the simulations of optical trapping assays; we did not incorporated the diffusive component of Ncd into the model, assuming that the diffusion takes place in the weakly bound states such as ADP state and thus is negligible when a load is imposed. The other differences from the low-load model are as follows. To simplify and reduce the calculations, we use a one-dimensional MT track. The motors are clustered at a single site on a bead. The attachment site on the MT is determined within a circular area of radius L, the distance between motor domains and the bead surface, which we assumed to be about 27 nm. We update the states and positions of the motors simultaneously for each time step. The motors can be attached to the same binding site on the MT, unlike the two-dimensional model. As a read-out for transport, the position of the bead is recorded. The position of the bead is determined by the applied force and thermal motion of the bead. The current position at time step t is

$$x(t) = x(t-1) + x_{\mathrm{random}} + x_{\mathrm{drift}},$$

where x_{random} is random step of the bead that is drawn from a Gaussian distribution with mean-square displacement $2D\Delta t$, and $x_{\mathrm{drift}} = (f/\gamma)\Delta t$, is the deterministic drift. The net force f is the sum of the trapping force $-kx$ (k, trap stiffness) and the restoring force $\sum_i(\kappa \times \Delta l_i)$ (κ, the linkage stiffness; Δl_i, the extension of the linkage between the bead and ith motor). The diffusion coefficient D is related to the friction constant γ according to the Einstein relation $\gamma = k_{\mathrm{B}}T/D = 6\pi\eta R$, where k_{B} is Boltzmann constant, T is absolute temperature, η is the viscosity of the medium, and R is the radius of the bead. According to the Faxén's law, the friction constant of a sphere with radius R whose center is a distance h

from the surface is

$$\gamma' = \frac{6\pi\eta R}{1 - \frac{9R}{16h} + \frac{R^3}{8h^3} - \frac{45R^4}{256h^4} - \frac{R^5}{16h^5}}.$$

We assume that the viscosity of the medium η is equal to that of water (0.914×10^{-21} N s nm^{-2} at 24°C), and the beads are positioned just on the glass surface for simplicity.

Algorithm for scanning parameter space

Simulated annealing algorithm offers rapid scanning of parameter space. The program randomly searches the parameters that minimize the sum of residuals between experimental and simulated data by heuristic algorithm, avoiding getting stuck at local minima.

The outline of the algorithm:

Initial parameters are randomly generated within a specified range.

1. Randomize the parameter set according to current temperature T. Each parameter is randomly increased, decreased, or unchanged by the step size calculated as $\log(T) \times$ specified unit step size in a specified range.
2. Perform the simulation with the newly generated parameter set.
2. If the sum of residuals between experimental and simulated data (ΔE) is smaller than the current one, then accept the new parameter set and go to step 4.
3. Even if the new parameter set gave a worse result, accept the new parameters depending on the probability

$$P = \exp\left(\frac{-|\Delta E|}{T}\right).$$

4. If the new parameter set is best ever, save the new one as the best parameter set.
5. Decrease the temperature by a specified rate (cooling factor; typically, 0.995–0.997).
6. If the temperature reaches lower bound ($T_{\min}$= 0.001), report the best parameter set, else go to step 1.

Effects of the arrangement of two coupled kinesins

The in vitro experiment showed that run length of two coupled motors increased with closer

spacing except for two kinesin-1 motors linked by flexible linkers (Figs. 2C *right* and S12B). We hypothesized that there are two opposing factors that make the run length dependent on the spacing: (*i*) the on-rate of the tethered motor and (*ii*) the pulling forces between dimers via the linker. When the spacing is getting closer, the on-rate become higher, while the pulling forces are applied more frequently to each other, leading to load-induced detachment. Consequently, the run length would be determined by the balance of these two opposing factors. Because the effect on the on-rate is discussed in the main text, we focus here on the interactions between motors. The experimental observations show that the type of DNA linker affects the motility only when the spacing is small. This could be explained by the property of DNA linker. DNA can be described as an entropic spring and therefore is much stiffer when its contour length and persistence length is shorter. This feature leads to the counter-intuitive property that flexible DNA linkers (single stranded) are much stiffer than rigid DNA linkers (double stranded) particularly when their length is short (20). This is consistent with the general tendency of the run lengths of both kinesins to be shorter with flexible DNA linkers than those with rigid DNA linkers. On the other hand, there is large difference in the spacing-dependence of run length between kinesin-1 and Ncd. One possibility is the difference in the strength of motor−motor interactions; any tension between motors tends to be relaxed by the diffusive movement of Ncd, unlike kinesin-1. Moreover, there may be formerly unknown interference between kinesin-1 dimers, as proposed by Rogers *et al*. (26). Using two coupled kinesin-1 dimers linked by a 50-nm DNA duplex, the authors have proposed that asynchronous motor stepping and strain between motors lead to negative effect on motility when they are coupled via an elastic linker. They have reported that the run length of two coupled kinesin-1 dimers is 1.7-fold that of a single motor, which is smaller than our value of 2.4-fold. The difference is most likely due to the difference in the elastic components of the two constructs. These observations lead us to consider that the stiffness of linkage is important for coordination of coupled motors. Further work on more realistic modeling of the linker (including motor protein itself) is required to better describe these effects on collective motility.

Comparison with the MT landing experiment

A previous study suggested that at least four dimeric Ncds are needed for continuous MT gliding (27). In MT gliding assays, Ncd dimers are immobilized on the glass surface and randomly distributed

over the surface. When small numbers of Ncd interact with a MT, spacing between motors on average is probably much larger than that in our assays. This makes difficult for Ncd to rebind the MT, given the spacing-dependence of the on-rate and the thermal diffusion of the MT. If two or three Ncd motors are clustered at single spot on the surface, it is likely that the landed MT can be continuously driven by the cluster of Ncd.

References

1. Rice S, *et al.* (1999) A structural change in the kinesin motor protein that drives motility. *Nature* 402(6763):778-784.
2. Pierce DW, Hom-Booher N, Otsuka AJ, & Vale RD (1999) Single-molecule behavior of monomeric and heteromeric kinesins. *Biochemistry* 38(17):5412-5421.
3. Bradford MM (1976) A rapid and sensitive method for the quantitation of microgram quantities of protein utilizing the principle of protein-dye binding. *Anal Biochem* 72:248-254.
4. Markham NR & Zuker M (2008) UNAFold: software for nucleic acid folding and hybridization. *Methods Mol Biol* 453:3-31.
5. Williams RC, Jr. & Lee JC (1982) Preparation of tubulin from brain. *Methods Enzymol* 85 Pt B:376-385.
6. Hyman A, *et al.* (1991) Preparation of modified tubulins. *Methods Enzymol* 196:478-485.
7. Yildiz A, *et al.* (2003) Myosin V walks hand-over-hand: single fluorophore imaging with 1.5-nm localization. *Science* 300(5628):2061-2065.
8. Furuta K & Toyoshima YY (2008) Minus-end-directed motor Ncd exhibits processive movement that is enhanced by microtubule bundling in vitro. *Curr Biol* 18(2):152-157.
9. Helenius J, Brouhard G, Kalaidzidis Y, Diez S, & Howard J (2006) The depolymerizing kinesin MCAK uses lattice diffusion to rapidly target microtubule ends. *Nature* 441(7089):115-119.
10. Thorn KS, Ubersax JA, & Vale RD (2000) Engineering the processive run length of the kinesin motor. *J Cell Biol* 151(5):1093-1100.
11. Qian H, Sheetz MP, & Elson EL (1991) Single particle tracking. Analysis of diffusion and flow in two-dimensional systems. *Biophys J* 60(4):910-921.
12. Iwaki M, Iwane AH, Shimokawa T, Cooke R, & Yanagida T (2009) Brownian search-and-catch mechanism for myosin-VI steps. *Nat Chem Biol* 5(6):403-405.
13. Nishiyama M, Muto E, Inoue Y, Yanagida T, & Higuchi H (2001) Substeps within the 8-nm step of the ATPase cycle of single kinesin molecules. *Nat Cell Biol* 3(4):425-428.
14. Ueno H, *et al.* (2010) Simple dark-field microscopy with nanometer spatial precision and microsecond temporal resolution. *Biophys J* 98(9):2014-2023.
15. Kojima H, Muto E, Higuchi H, & Yanagida T (1997) Mechanics of single kinesin molecules measured by optical trapping nanometry. *Biophys J* 73(4):2012-2022.

16. Tolić-Nørrelykke SF, *et al.* (2006) Calibration of optical tweezers with positional detection in the back focal plane. *Rev Sci Instrum* 77(10):103101.
17. Block SM, Goldstein LS, & Schnapp BJ (1990) Bead movement by single kinesin molecules studied with optical tweezers. *Nature* 348(6299):348-352.
18. Kunwar A, Vershinin M, Xu J, & Gross SP (2008) Stepping, strain gating, and an unexpected force-velocity curve for multiple-motor-based transport. *Curr Biol* 18(16):1173-1183.
19. Kunwar A & Mogilner A (2010) Robust transport by multiple motors with nonlinear force-velocity relations and stochastic load sharing. *Phys Biol* 7(1):16012.
20. Howard J (2001) *Mechanics of Motor Proteins and the Cytoskeleton* (Sinauer Associates, Inc., Sunderland, MA) 1st Ed.
21. Murphy MC, Rasnik I, Cheng W, Lohman TM, & Ha T (2004) Probing single-stranded DNA conformational flexibility using fluorescence spectroscopy. *Biophys J* 86(4):2530-2537.
22. Hagerman PJ (1988) Flexibility of DNA. *Annual review of biophysics and biophysical chemistry* 17:265-286.
23. Matsumoto M & Nishimura T (1998) Mersenne Twister: A 623-dimensionally equidistributed uniform pseudorandom number generator. *ACM Trans. on Modeling and Computer Simulation* 8(1):3-30.
24. deCastro MJ, Fondecave RM, Clarke LA, Schmidt CF, & Stewart RJ (2000) Working strokes by single molecules of the kinesin-related microtubule motor ncd. *Nat Cell Biol* 2(10):724-729.
25. Valentine MT, Fordyce PM, Krzysiak TC, Gilbert SP, & Block SM (2006) Individual dimers of the mitotic kinesin motor Eg5 step processively and support substantial loads in vitro. *Nat Cell Biol* 8(5):470-476.
26. Rogers AR, Driver JW, Constantinou PE, Kenneth Jamison D, & Diehl MR (2009) Negative interference dominates collective transport of kinesin motors in the absence of load. *Phys Chem Chem Phys* 11(24):4882-4889.
27. deCastro MJ, Ho CH, & Stewart RJ (1999) Motility of dimeric ncd on a metal-chelating surfactant: evidence that ncd is not processive. *Biochemistry* 38(16):5076-5081.

Figures and Movies

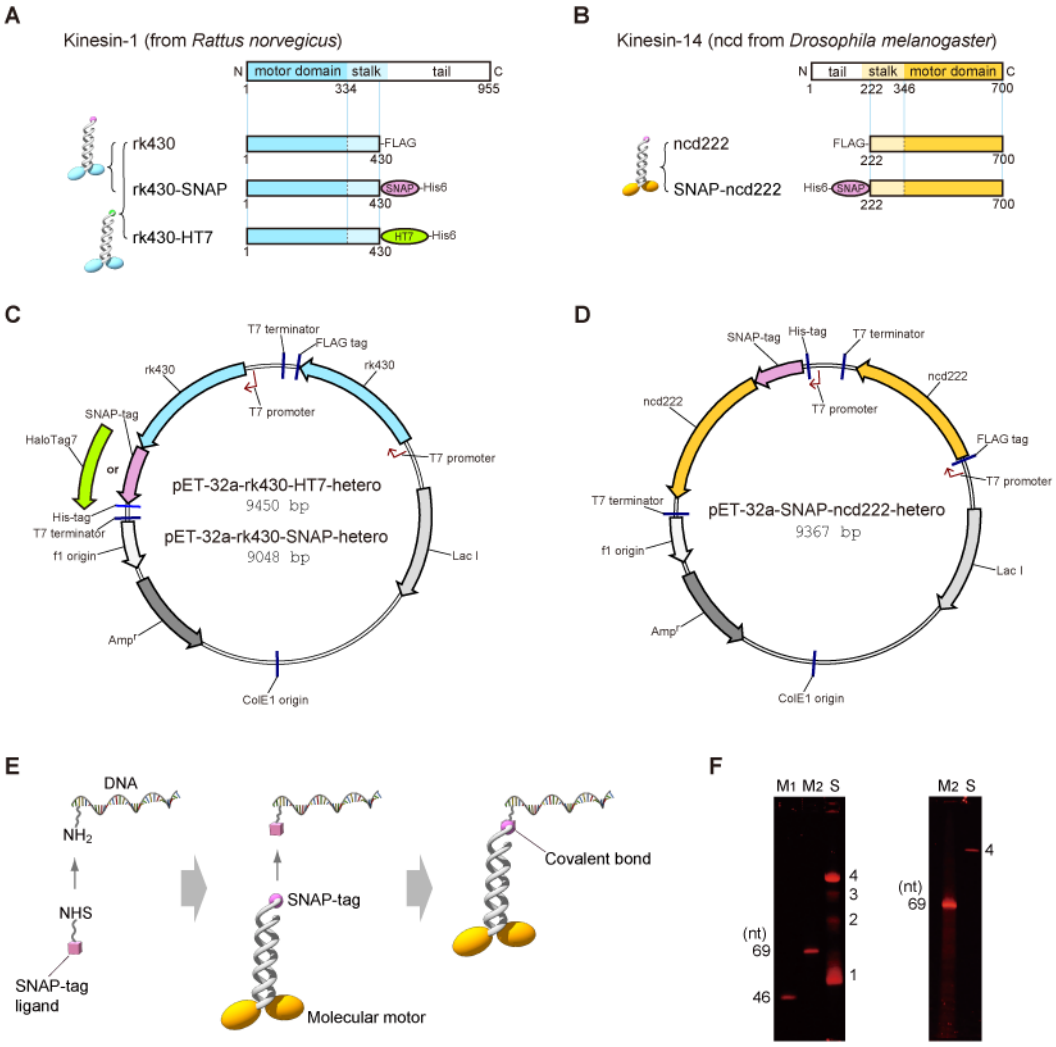

Fig. S1. Construction of DNA−motor assemblies

(A and B) Schematic representations of kinesin-1 (A) and Ncd (B) constructs. Full-length proteins are shown at the top.

(C and D) Diagrams of the vectors that express the heterodimer of kinesin-1 (C) and Ncd (D).

(E) Schematic illustration of DNA−motor construction.

(F) Purification of DNA scaffold. The ligated DNA sample was separated by denaturing polyacrylamide gel electrophoresis (10% acrylamide / 7 M urea gel, *left*). After purification, the purity of the DNA scaffold composed of four DNA fragments was checked by PAGE analysis (*right*). The Cy5 dyes attached to the DNA scaffold were excited by 617-nm LED illumination and captured by CCD camera through a 665-nm long-pass filter. Abbreviations: M_1, marker 1 (46 nt);

M_2, marker 2 (69 nt); S, DNA sample.

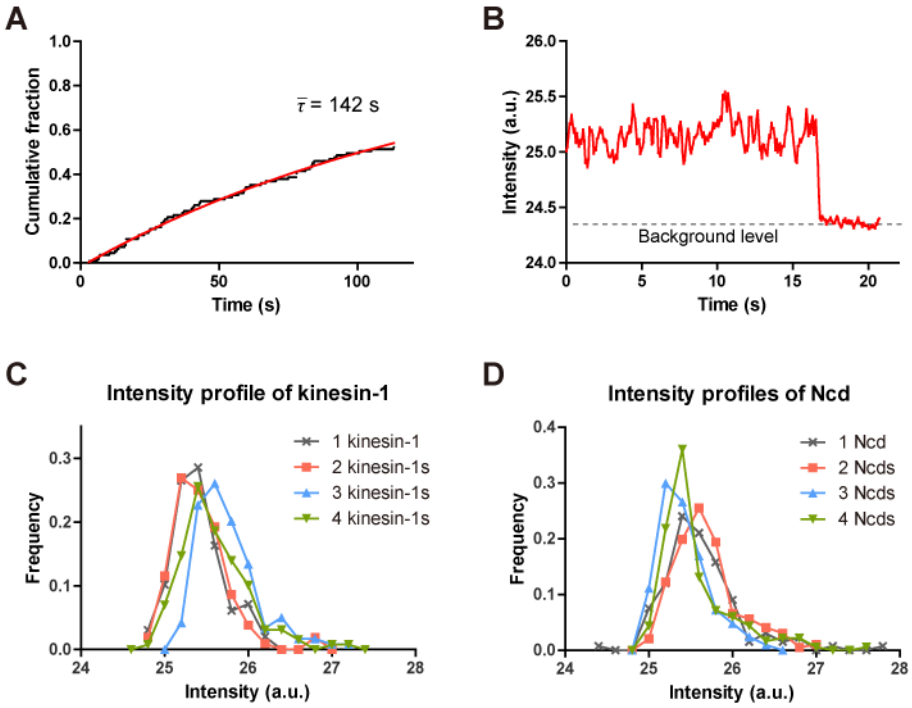

Fig. S2. Observation of the fluorescent probe attached to DNA scaffolds

(A) Estimation of the bleaching rate of Cy5 dye. The Cy5 dyes attached to DNA scaffolds were immobilized on the glass surface. The plot in black shows the cumulative histogram of the duration before bleaching. The mean duration was determined by using nonlinear fitting of the cumulative fraction $1 - \exp(-t/\tau)$ (red plot).

(B) Representative trace of photobleaching behavior of single Cy5 dyes attached to DNA scaffolds. One-step photobleaching events were clearly observed. The dashed line represents the background level.

(C and D) Intensity profiles of moving kinesin-1 and Ncd, respectively. Fluorescence intensities of moving spots are plotted as histograms. The profiles show that the moving spots corresponded to single Cy5 dyes, excluding the possibility of aggregation and undesired hybridization.

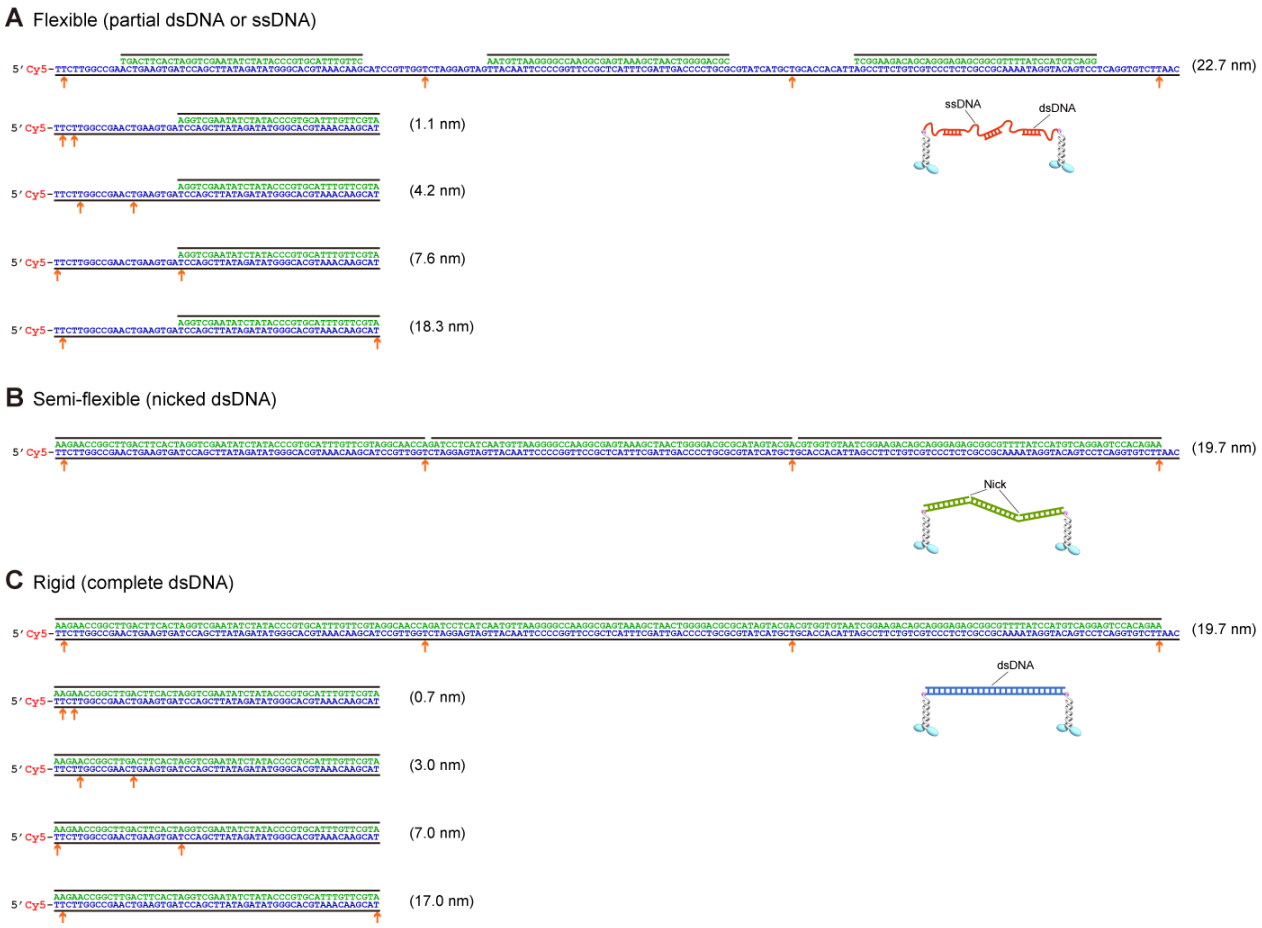

Fig. S3. Schematic representation of DNA scaffolds used for motility assays at low load

(A, B, and C) Layout of the DNA strands and modified bases for flexible (A), semi-flexible (B), and rigid (C) DNA scaffolds. Arrows denote the amino modified bases (ligand binding sites). Values in parentheses represent average spacing calculated from the end-to-end distance of DNA between two amino modified bases.

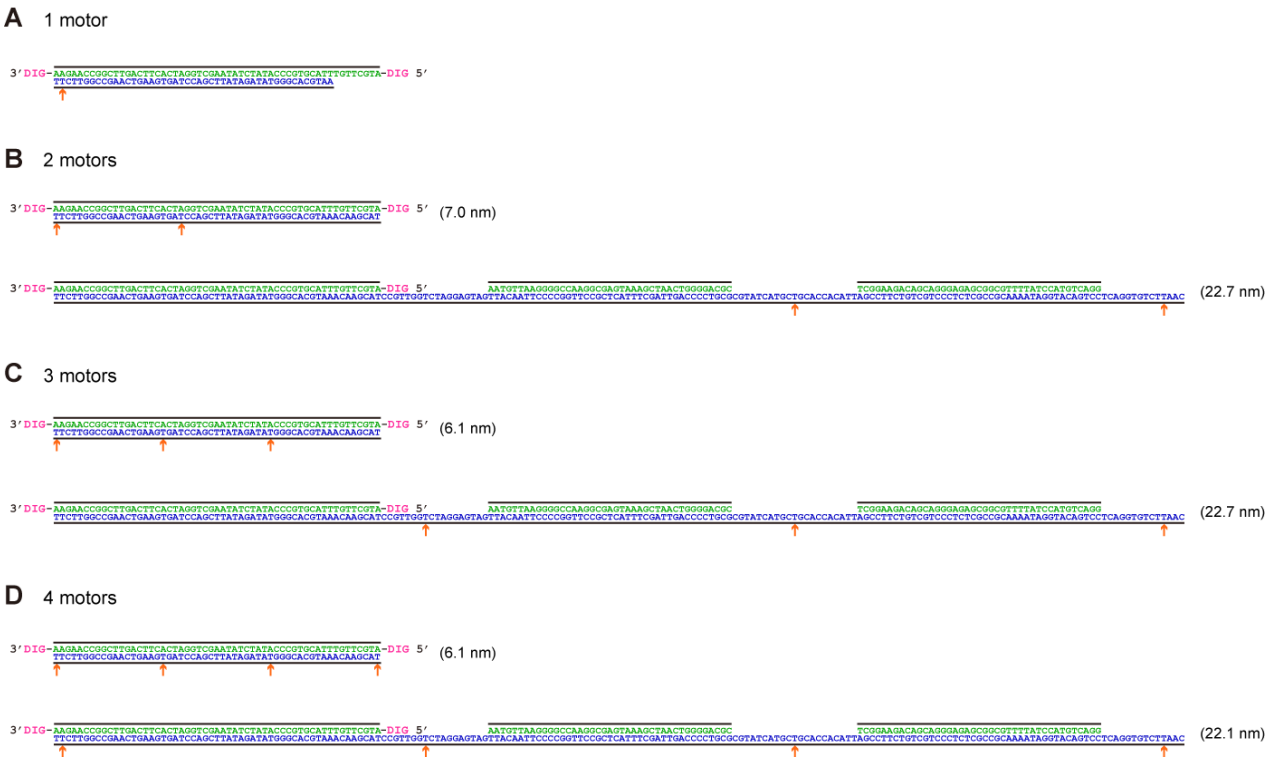

Fig. S4. Schematic representation of DNA scaffolds used for optical trapping

(A, B, C, and D) Layout of the DNA strands and modified bases for one to four motors. Arrows denote the amino modified bases. “DIG” in magenta refers to a digoxigenin molecule introduced during oligomeric DNA synthesis. Values in parentheses represent average spacing calculated from the end-to-end distance of DNA between two amino modified bases.

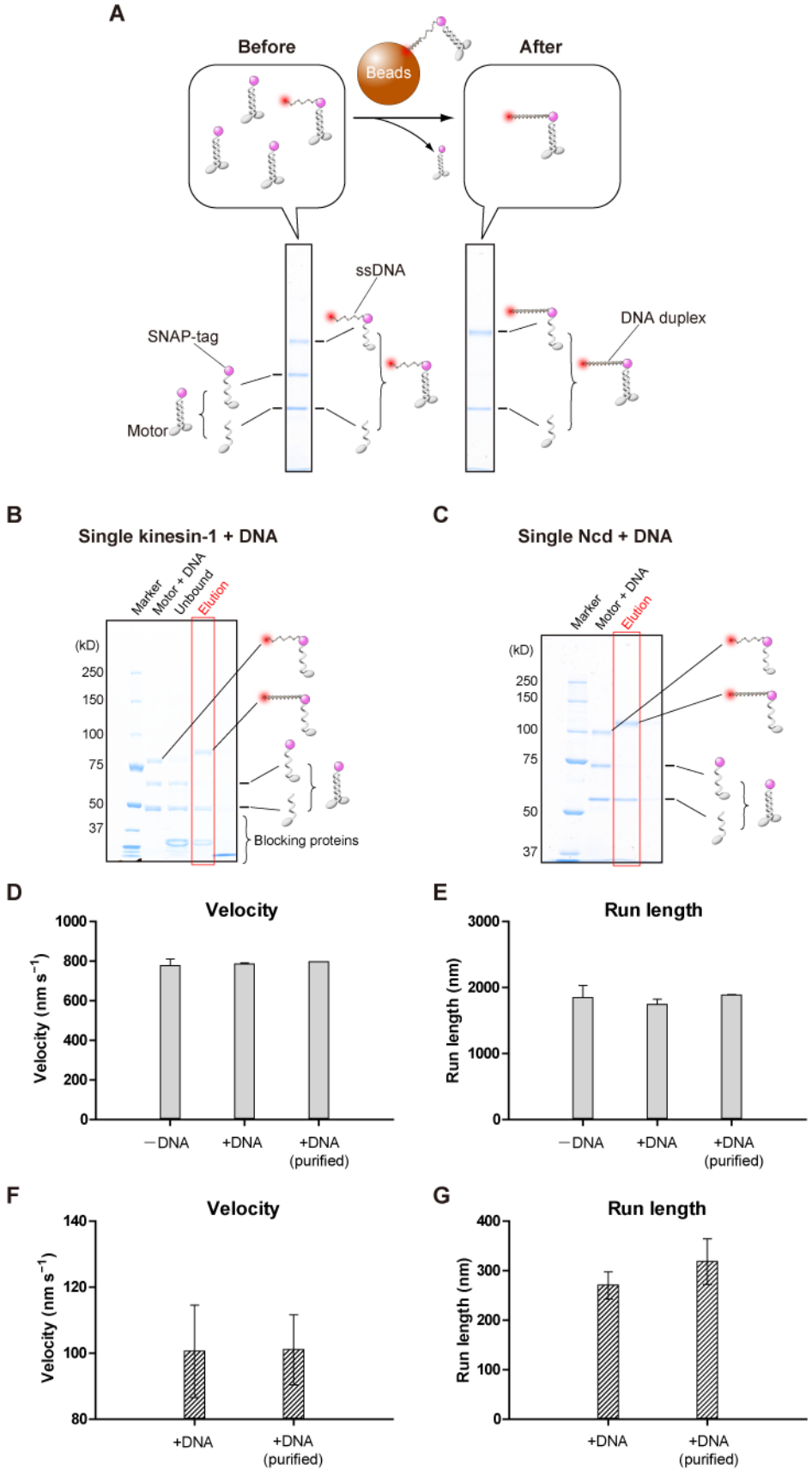

Fig. S5. Motility of single kinesin-1 and Ncd motors with and without an excessive amount of

motors

(A) Schematic of the purification process.

(B and C) SDS-PAGE analysis of the removal of free kinesin-1 (B) or Ncd (C) molecules in the solution. SDS-PAGE was performed on a 3–10% (B) or 10% (C) polyacrylamide gel that was stained with Coomassie Brilliant Blue G-250-based reagent after electrophoresis. Note that the eluate of kinesin−DNA contains a protein-based blocking reagent to avoid nonspecific binding to the magnetic beads.

(D and E) Motility of single kinesin-1 motors. Bars represent mean ± SEM. The total numbers of runs were 156, 175, and 151 for −DNA, +DNA, and +DNA (purified), respectively. “Purified” represents removal of an excess amount of free motors. The purification was performed by using DNA-conjugated magnetic beads (see *p*.5).

(F and G) Motility of single Ncds. The total numbers of scored runs were 133 and 86 (the detected binding events were 449 and 381) for +DNA and +DNA (purified), respectively.

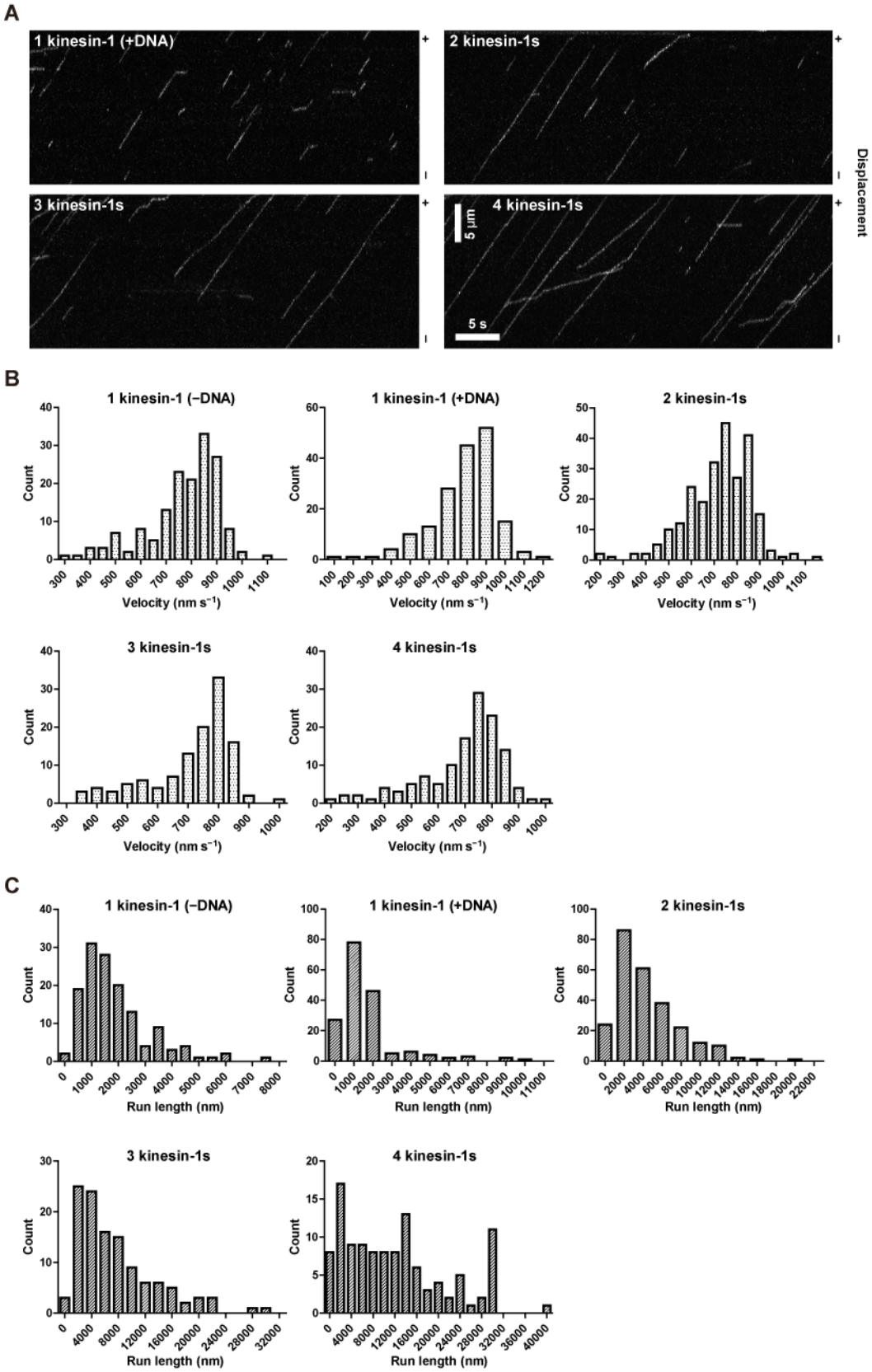

Fig. S6. Collective motility of multiple-kinesin-1 assemblies (experiment)

(A) Kymographs showing the motion of the assemblies including 1, 2, 3 or 4 kinesin-1 dimer(s) on

flexible DNA scaffolds. Plus (+) and minus (–) symbols on the right of the kymographs refer to the polarity of the MT.

(B and C) Histograms of velocity (B) and run length (C).

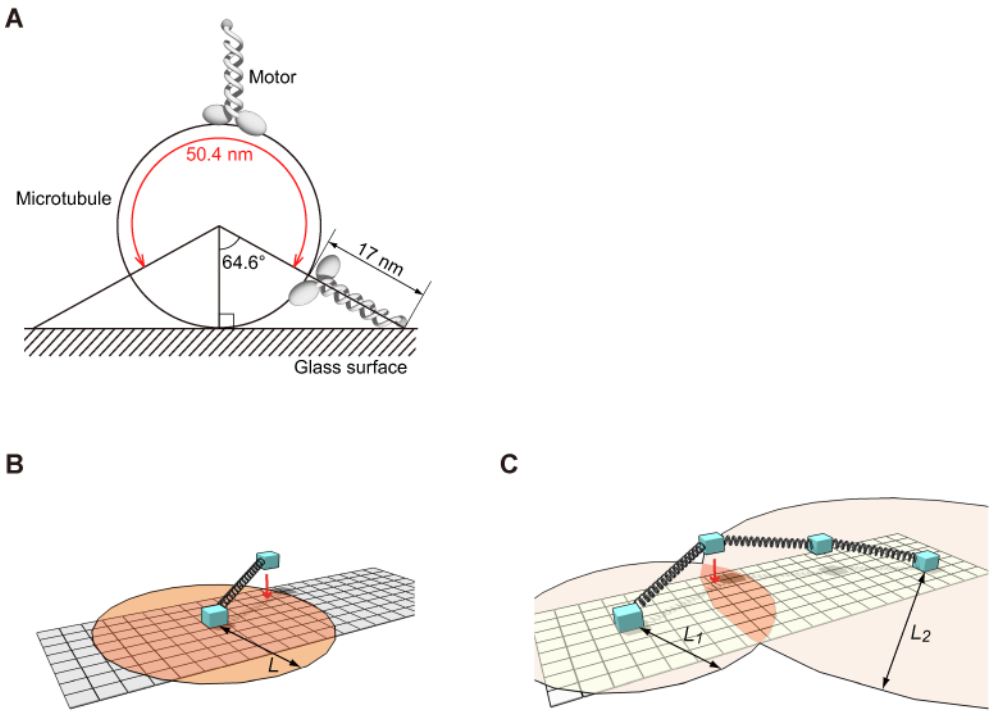

Fig. S7. Schematic illustration of how MT width and binding sites on a MT were determined for simulation

(A) The MT width was determined based on a geometric configuration in which kinesin with a 17-nm length does not interfere with a glass surface. The calculated width of 50.4 nm was rounded off to the nearest multiple of 6 nm, i.e., 48 nm. The diameter of MT was assumed to be 25 nm. (B) The motor to be bound can access any binding site within the circular area of radius *L* while tethered to the track via a single linker of end-to-end length *L*. (C) The motor to be bound is tethered to the track via two linkers. The motor can access binding sites within the overlapped region of the circular areas of radius L_1 and L_2, the end-to-end length of the DNA linkers.

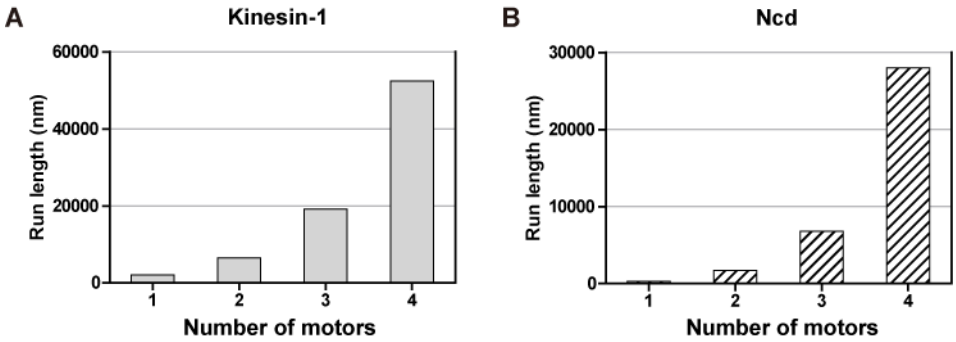

Fig. S8. Run lengths of single kinesin-1 and Ncd motors on extremely long MTs (simulation)

(A and B) The length of the MT was set to 10 mm (not 10 μm). Each plot represents the mean of 3000 traces.

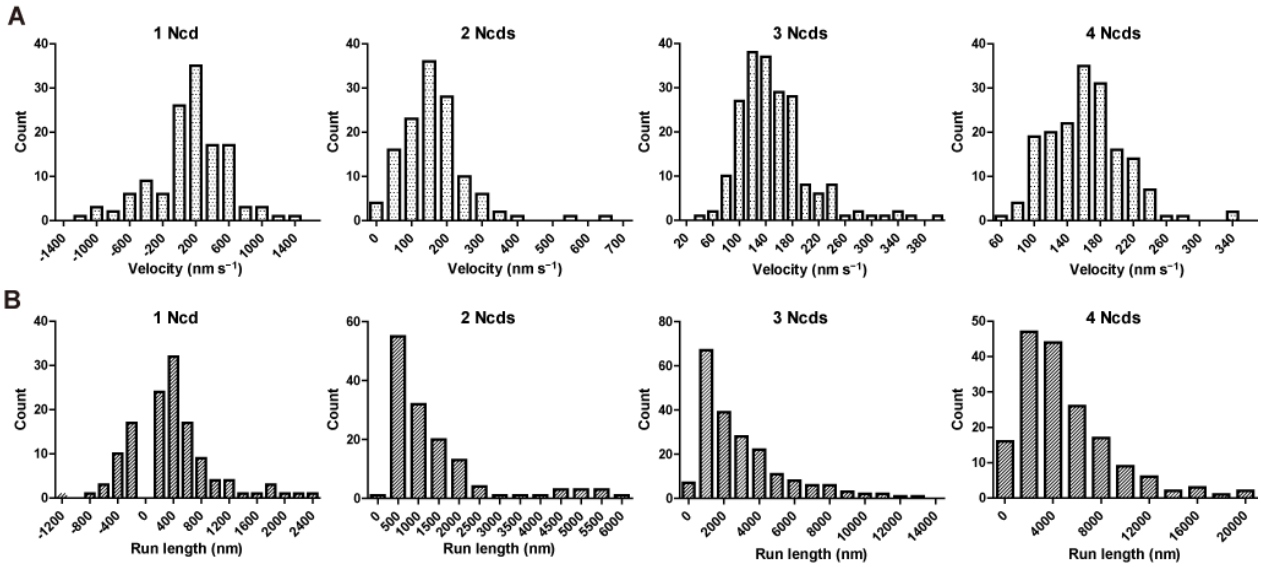

Fig. S9. Velocities and run lengths of multiple–Ncd assemblies (experiment)

(A and B) Histograms of velocity (A) and run length (B).

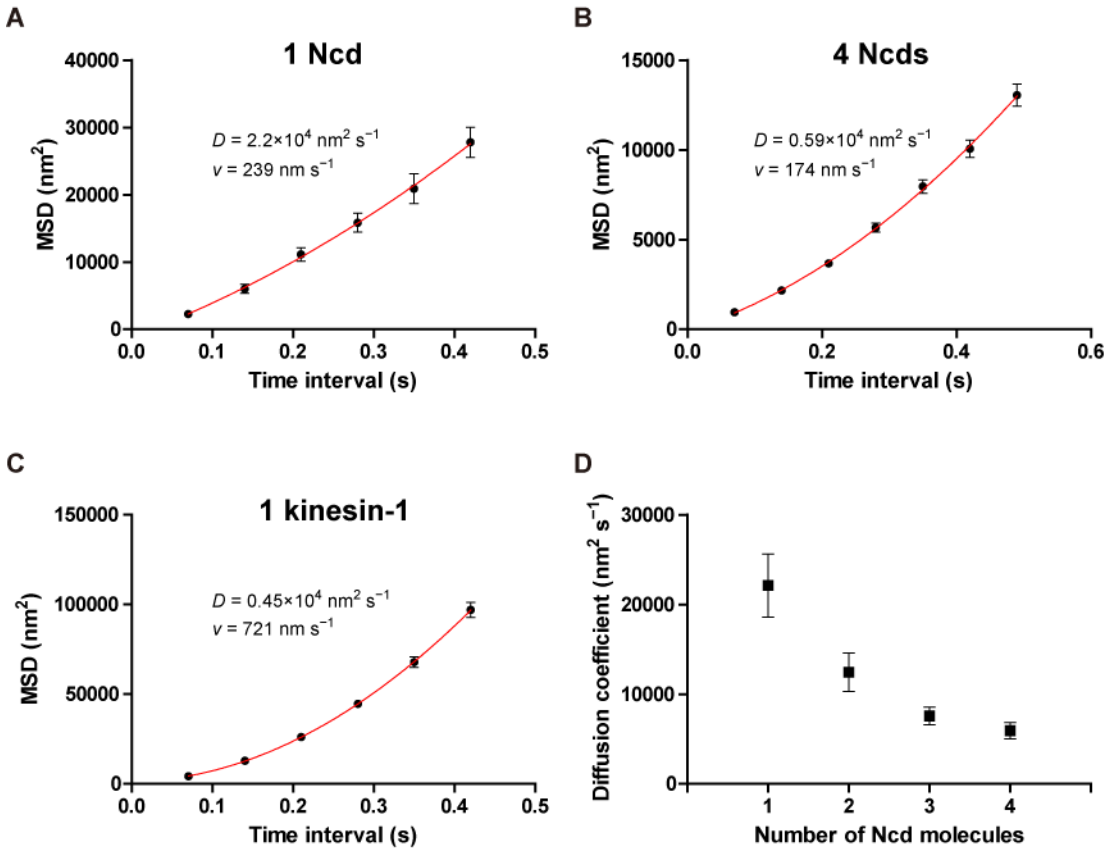

Fig. S10. MSD plots and diffusion coefficient (experiment)

(A–C) MSD plots of the assemblies including single Ncd (A), four Ncds (B), and single kinesin-1 (C) with the fitted quadratic curves. (D) Diffusion coefficients of the assemblies including 1, 2, 3, or 4 Ncd dimer(s) along MTs. Each plot represents mean ± SEM.

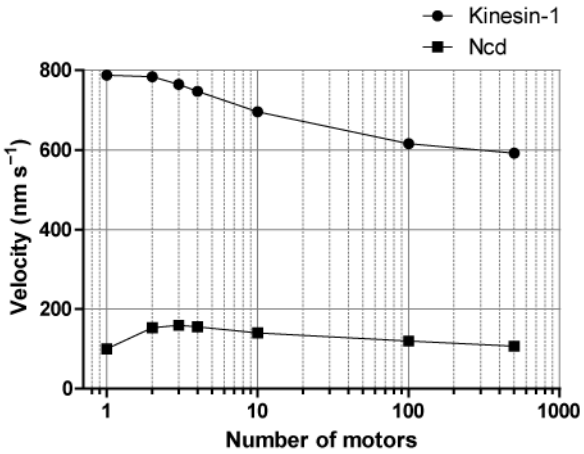

Fig. S11. Velocities of multiple kinesin-1 and Ncd motors (simulation)

The motors are linked by flexible DNA scaffolds (22.7-nm spacing). Each plot (circles, kinesin-1; squares, Ncd) represents the mean of 2000 traces except for the cases of 100 and 500 motors that were calculated from 500 traces.

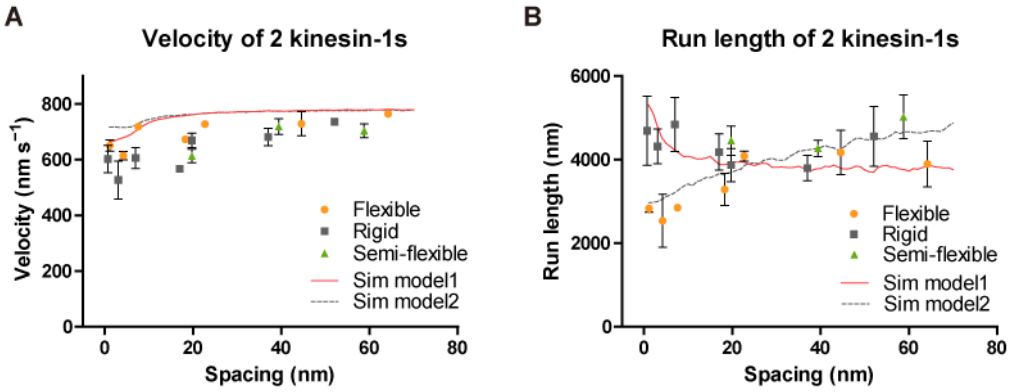

Fig. S12. Effects of the arrangement of two coupled kinesin-1 dimers (experiment)

Velocities (A) and run lengths (B) of two coupled kinesin-1 dimers. Color scheme, symbol, and simulation models are same as in Fig. 2C.

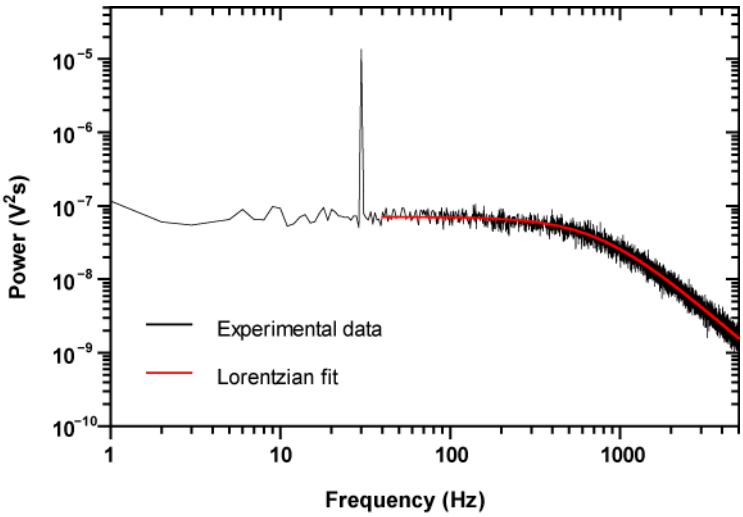

Fig. S13. Power spectrum of a 0.45-μm diameter bead held in the optical trap

The stage was driven with amplitude 218 nm at 30 Hz. The power spectrum is the average of 34 independent power spectra, which consists of a thermal noise (corner frequency = 751.5 Hz) and

a calibration spike at 30 Hz (peak height = 1.34×10^{-5} V^2s). Fast Fourier transform was performed using a rectangular window (LabVIEW 8.5, National Instruments). The data at f < 40 Hz are excluded from the Lorentzian fit. The measurement time for each spectrum was 1 s, and the temperature was 24°C. These data gave the trap stiffness of 0.0174 pN nm^{-1} and solvent viscosity 8.68×10^{-4} Pa s. On the other hand, the positional variance of the bead with the equipartition theorem gave the trap stiffness of 0.0169 pN nm^{-1}.

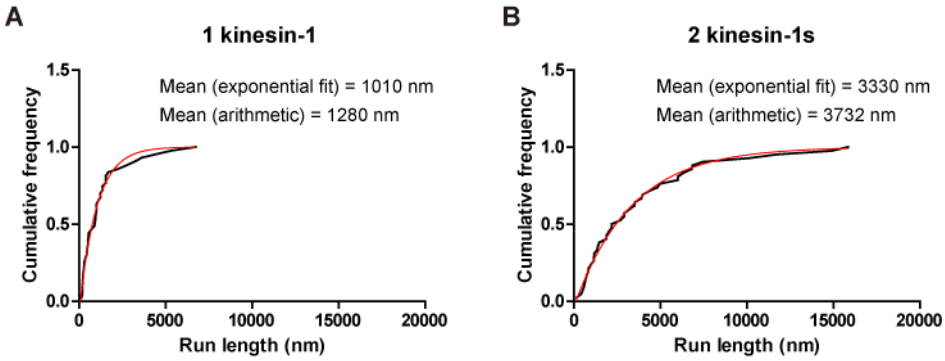

Fig. S14. Run lengths of kinesin-1–bead in the absence of a trapping force (experiment)

(A and B) Cumulative histogram of kinesin-1–beads driven by single kinesin-1 motors (A) and two coupled kinesin-1 motors (B). The total numbers of runs were 43 and 42 for single and two coupled kinesin-1 motors, respectively. Mean values were calculated from two methods. One was calculated from the arithmetic mean, and the other was determined by using nonlinear fitting of the cumulative fraction $1-\exp\{(x_0-x)/\bar{x}\}$ (red plot). Although exponential fit may not be appropriate for two coupled kinesin-1 motors, cumulative frequency and the identical exponential model fitting were used to compare the run lengths of two assemblies to avoid the effect of inaccuracy in measurements for short runs. Two methods gave parallel results and both values show the additive run length of two kinesin-1 motors compared to single kinesin-1 motors.

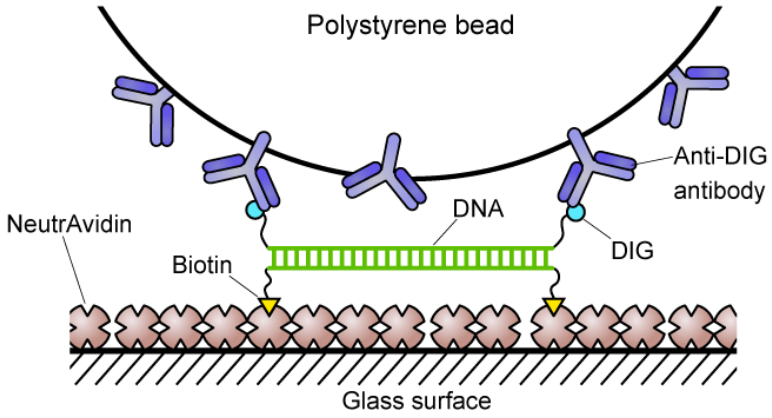

Fig. S15. Schematic of the control experiment for optical trapping

Polystyrene bead (0.45 μm in diameter) is tethered to the glass surface via NeutrAvidin, biotin, DNA duplex, digoxigenin (DIG), and anti-DIG antibody. The DNA duplex portion is illustrated as a ladder in green. We never observed unbinding of the beads from the surface with a trap stiffness of up to 0.3 pN nm^{-1}.

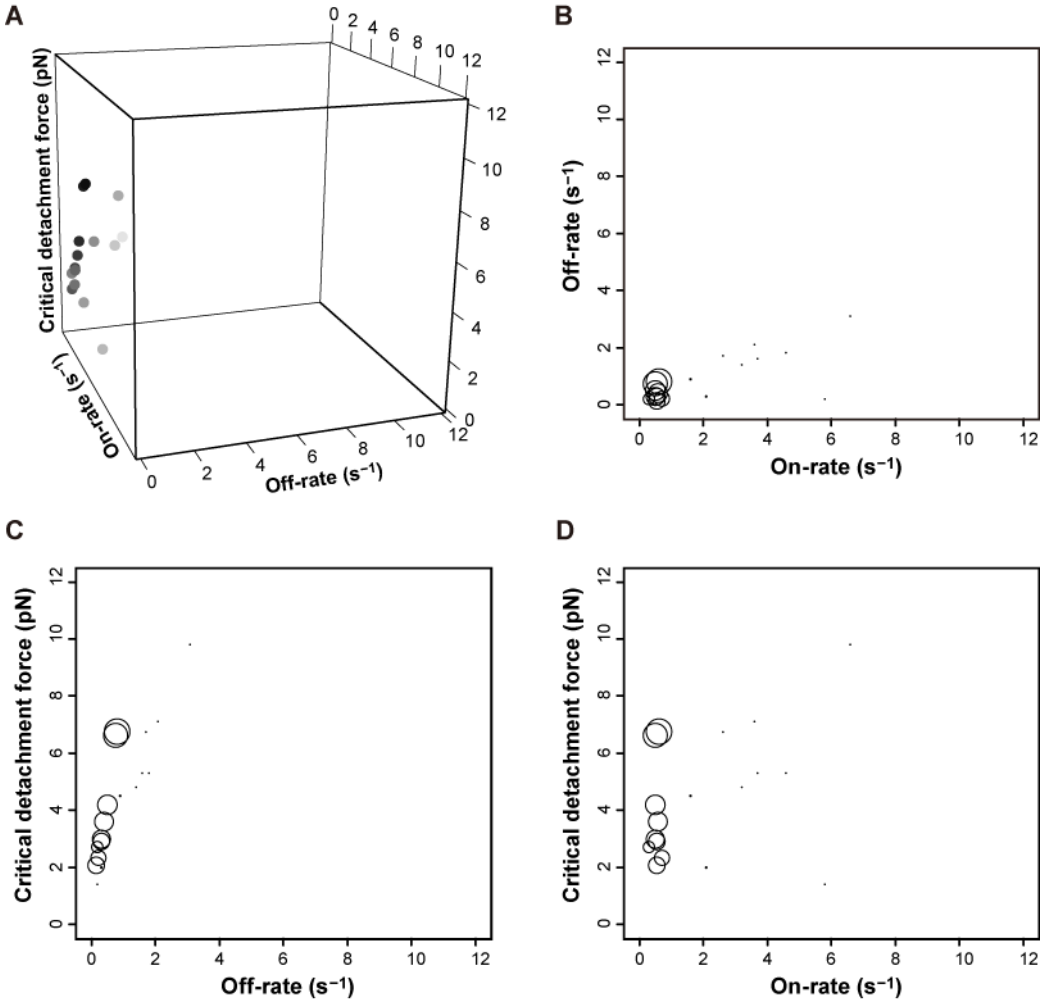

Fig. S16. Fitted parameters for optical trapping assays (kinesin-1)

(A) Three-dimensional plot of the fitted parameters. Each plot represents the parameter set obtained from different initial parameters. The darkness of the plot corresponds to the goodness of fit. The grayscale color map was equally divided by the number of plots and then assigned to each plot according to the sum of residuals between experimental and simulated data. Simulation parameters: linkage stiffness, 0.25 pN nm^{-1}; linker length, 27.0 nm; stall force, 6.8 pN; scale factor for critical detachment force (backward/forward), 1.0; stepping rate, 98.3 s^{-1}; force−velocity relationship, 2.0; bead diameter, 0.45 μm; trap stiffness, 0.025 pN nm^{-1}. Scanning conditions: initial temperature, 300.0; cooling factor, 0.995; unit step size, 0.1.

(B to D) Two-dimensional representations of (A). The size of the circles represents the goodness of fit, which is inversely proportional to the sum of residuals between experimental and simulated data.

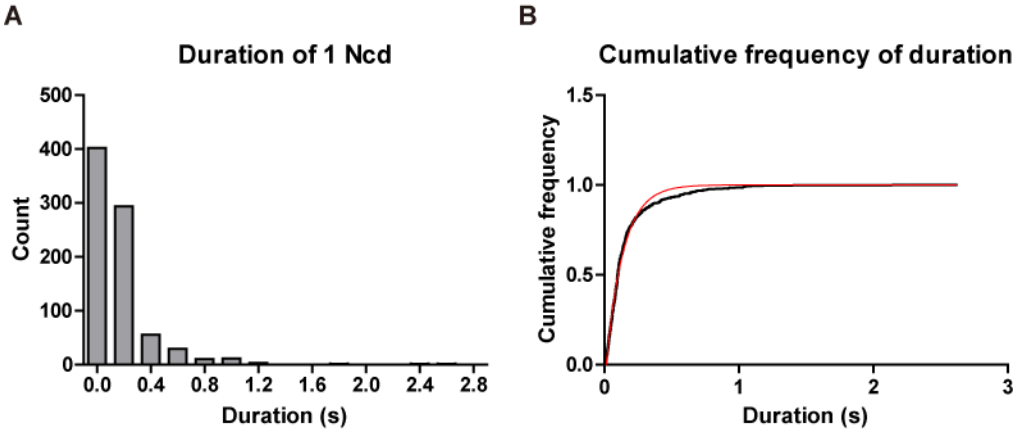

Fig. S17. Duration histogram of single Ncd−beads (optical trapping)

(A) Histogram of the duration. Each duration was determined manually from the time traces of trapped Ncd-beads by measuring the period of time between the binding and unbinding events on MTs. (B) Cumulative histogram of the same data as in (A). Mean value of the duration τ (0.128 s) was determined by using nonlinear fitting of the cumulative fraction $1 - \exp\{(x_0 - x)/\tau\}$ (red plot). Assay conditions: bead diameter, 0.21 μm; trap stiffness, 0.015 pN nm^{-1}; total count of binding event, 806; ATP, 1 mM.

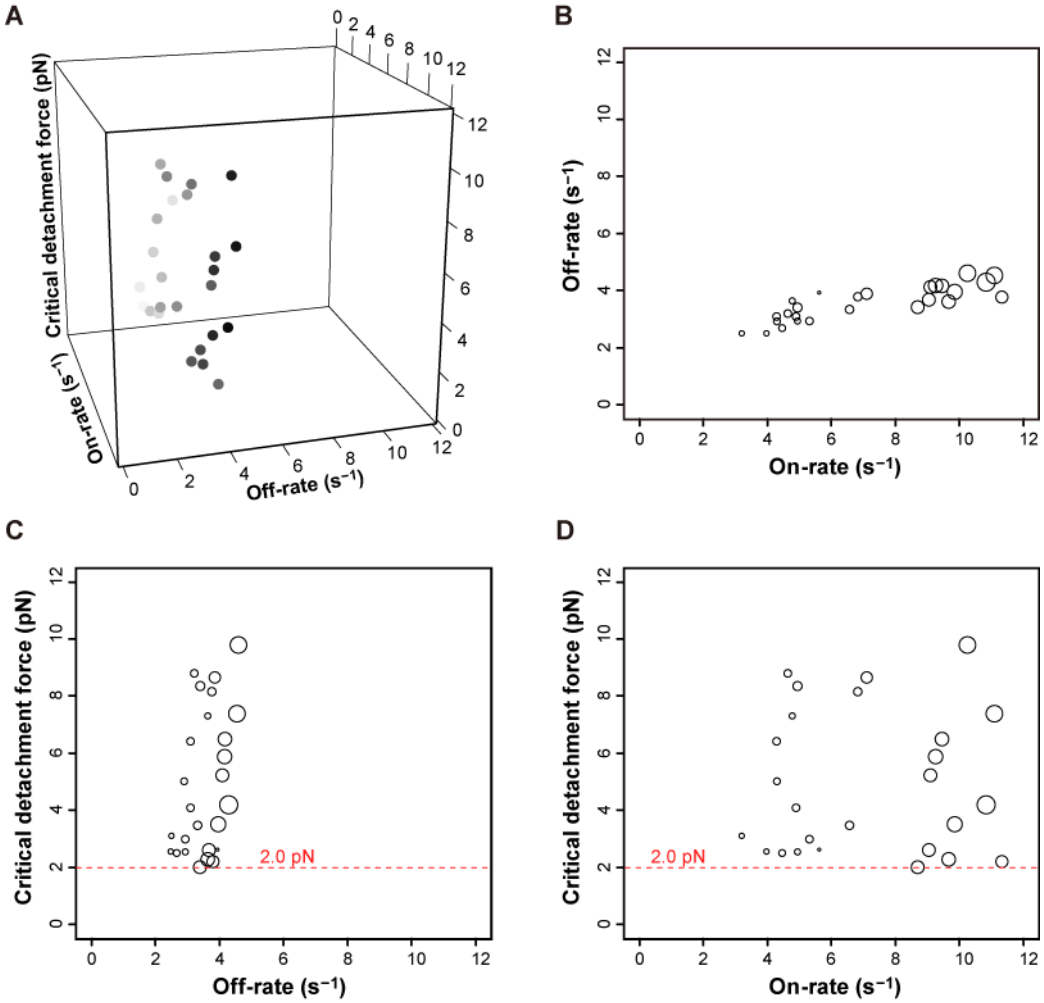

Fig. S18. Fitted parameters for optical trapping assays (Ncd)

(A) Three-dimensional plot of the fitted parameters. Each plot represents the parameter set obtained from different initial parameters. The color scheme is same as in Fig. S16. Simulation parameters: linkage stiffness, 0.25 pN nm^{-1}; linker length, 27.0 nm; stall force, 0.2 pN; scale factor for critical detachment force (backward/forward), 1.3; stepping rate, 22.0 s^{-1}; force−velocity relationship, 1.0; bead diameter, 0.21 μm; trap stiffness, 0.015 pN nm^{-1}. Scanning conditions: initial temperature, 300.0; cooling factor, 0.997; unit step size, 0.1.

(B to D) Two-dimensional representations of (A). The size of the circles represents the goodness of fit, which is inversely proportional to the sum of residuals between experimental and simulated data.

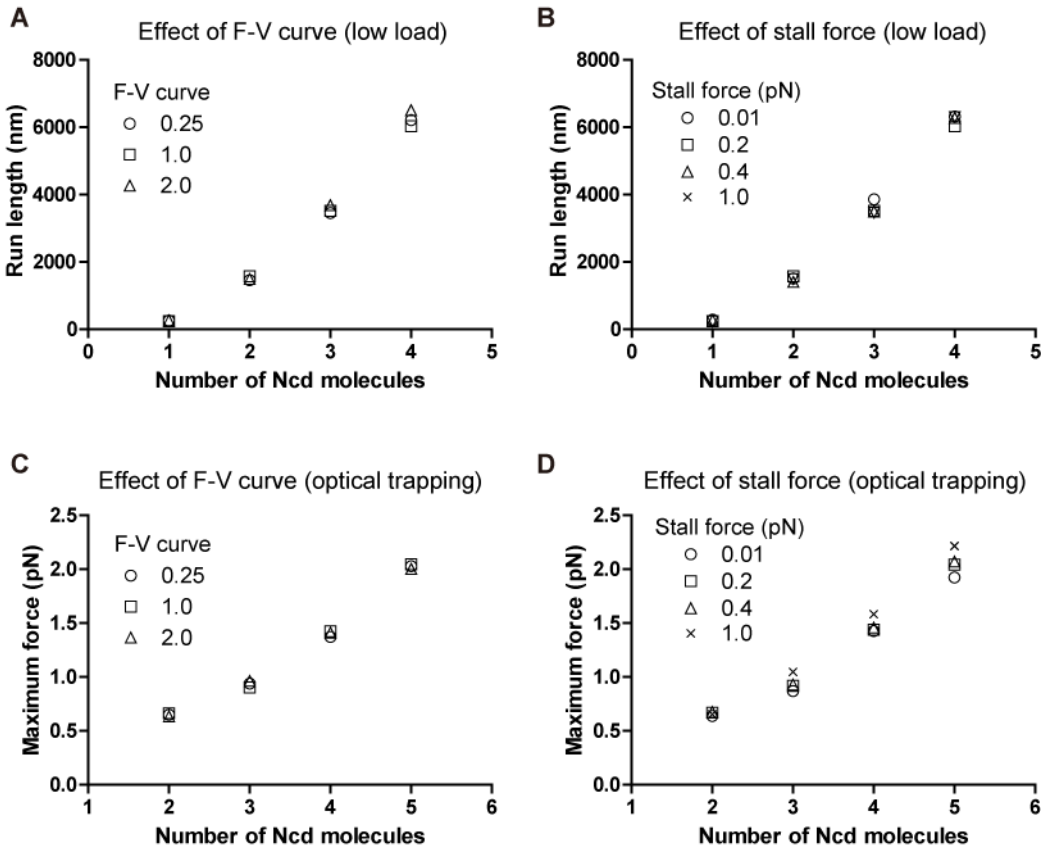

Fig. S19. Effect of the force−velocity curve and stall force on the motility of Ncd (simulation)

(A and B) Run lengths were plotted against the number of Ncd molecules with varying F−V curve *w* (A) and stall force F_s (B), respectively. Other parameters are listed in Table S6. Number of traces, 400 each.

(C and B) Average maximum forces plotted against the number of Ncd molecules with varying F-V curve *w* (C) and stall force F_s (D), respectively. Other parameters are listed in Table S7 (#2). Bead diameter, 0.21 μm; trap stiffness, 0.015 pN nm^{-1}; number of traces, 400 each.

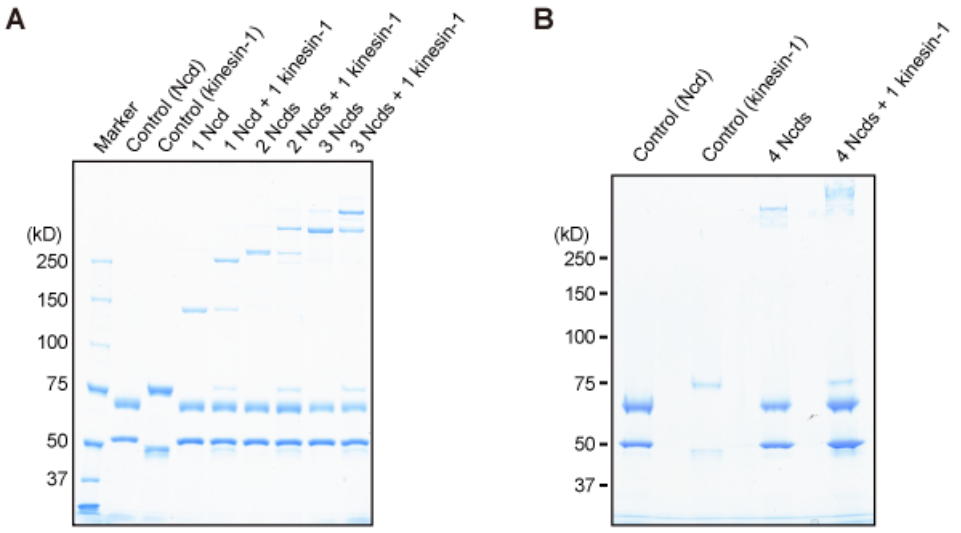

Fig. S20. SDS-PAGE analysis of constructs for tug-of-war between single kinesin-1 and several Ncds

(A-B) SDS-PAGE was performed on a 3–10% polyacrylamide gel that was stained with Coomassie Brilliant Blue G-250-based reagent after electrophoresis.

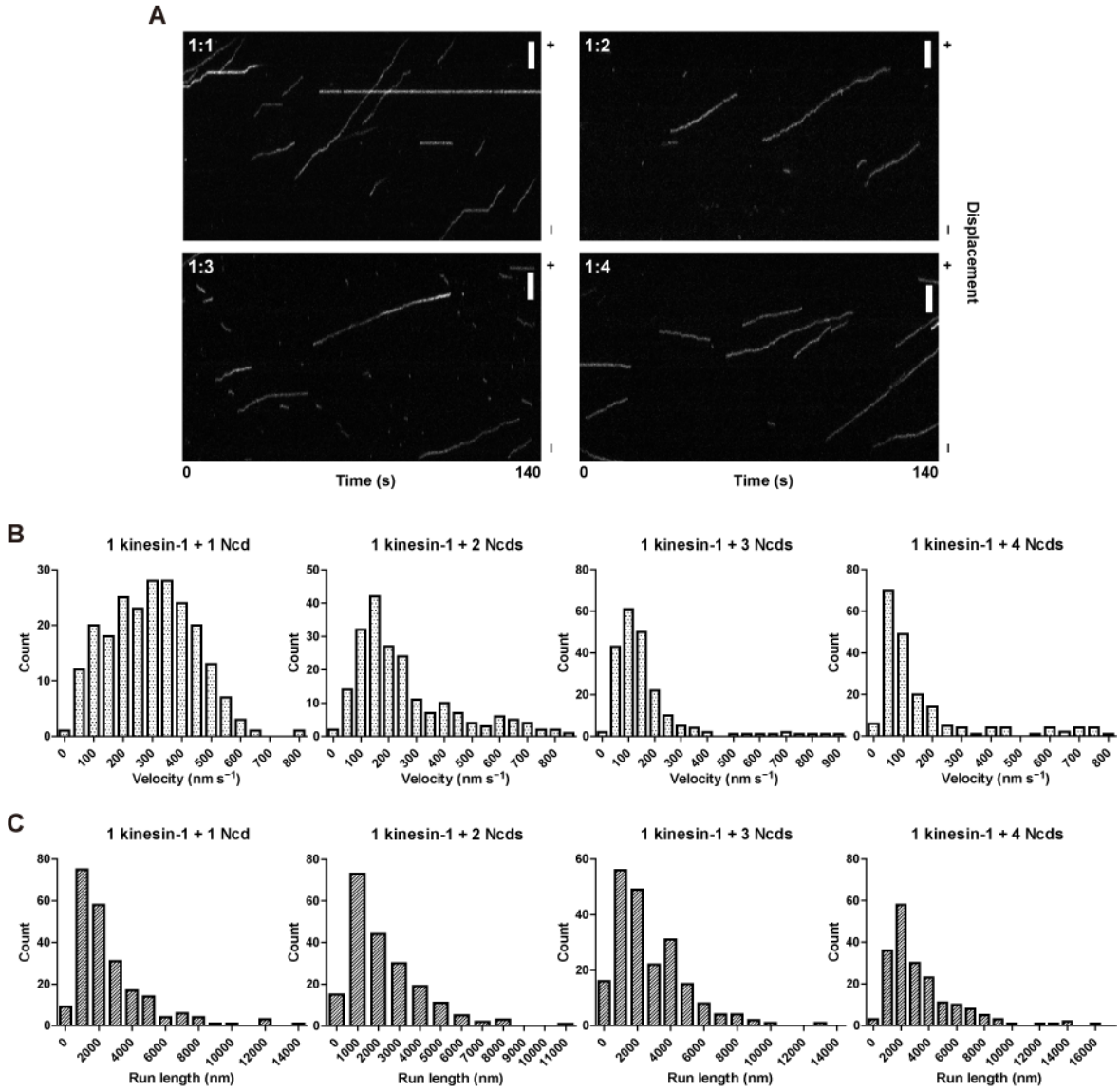

Fig. S21. Tug-of-war between single kinesin-1 and several Ncds (experiment)

(A) Kymographs showing the motion of the tug-of-war between a single kinesin-1 and 1, 2, 3 or 4 Ncd(s) on flexible DNA scaffolds. Plus (+) and minus (–) symbols on the right of the kymographs refer to the polarity of the MT. Scale bars, 3 μm.

(B and C) Histograms of velocity (B) and run length (C).

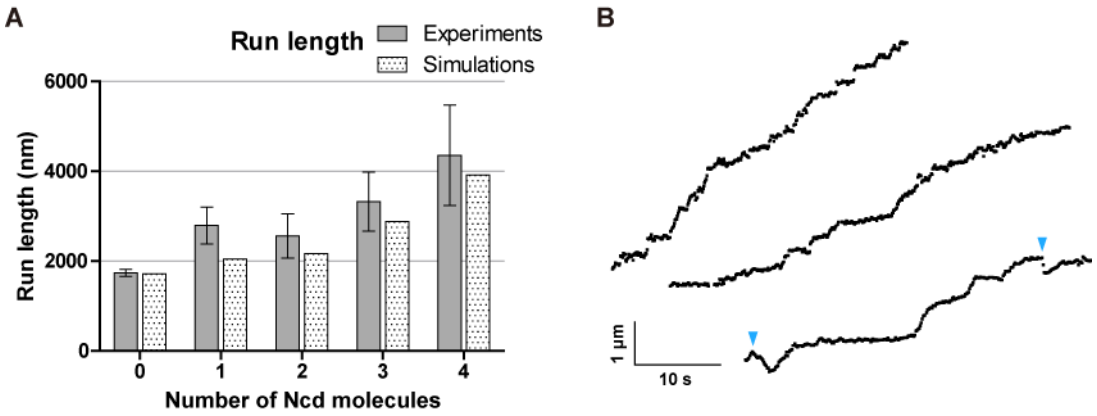

Fig. S22. Average run lengths and typical traces of tug-of-war between single kinesin-1 and several Ncds

(A) Run lengths of tug-of-war between single kinesin-1 and several Ncds. The parameter sets for simulation are shown in Table S5.

(B) Example traces of single kinesin-1 versus three Ncds (experiment). Each trace generally moved toward the MT plus end. Arrowheads indicate directional switching. The experimental trajectories were obtained from frame-averaged movies (4 frames).

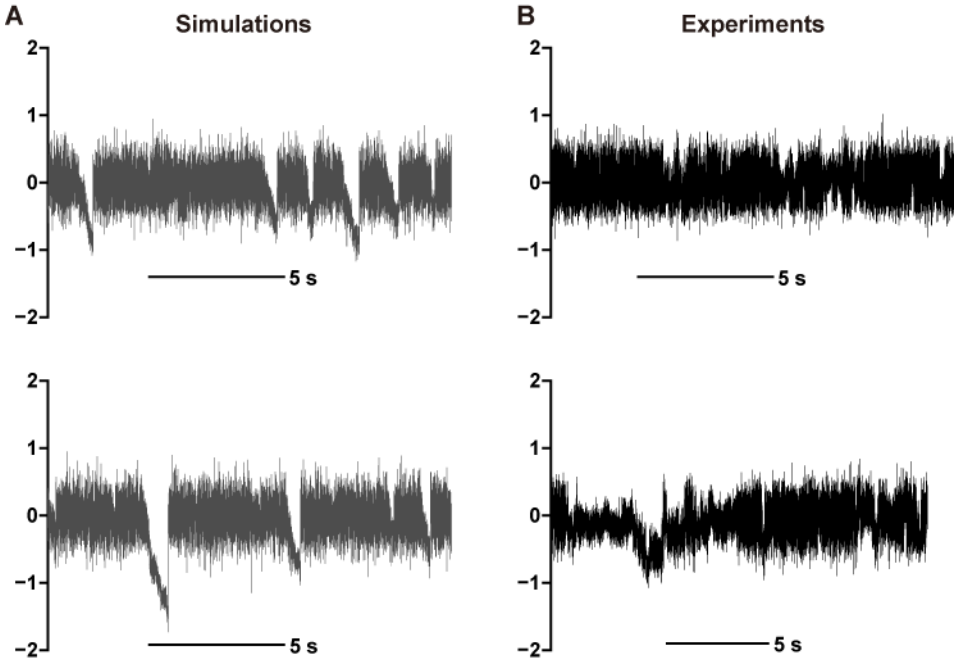

Fig. S23. Time traces of optical trapping assays for single Ncd motors

(A) Simulation parameters: linkage stiffness, 0.25 pN nm^{-1}; linker length, 27.0 nm; on-rate, 9.7

s^{-1}; off-rate, 3.6 s^{-1}; critical detachment force (backward), 2.96 pN; critical detachment force (forward), 2.3 pN; stall force, 0.2 pN; stepping rate, 22.0 s^{-1}; trap stiffness, 0.015 pN nm^{-1}. All of the binding events were included to make simulated time traces without placing the detection limit for the maximum force.

(B) Assay conditions: bead diameter, 0.21 μm; trap stiffness, 0.015 pN nm^{-1}; ATP, 1 mM.

Table S1. Collective Motility of Kinesin-1 and Ncd

Motor Protein	Number of Motors	Velocity (nm s^{-1})	Run Length (nm)	MT Length (nm)	Diffusion coefficient ($\times 10^4$ nm^2 s^{-1})	n
Kinesin-1						
	1 (−DNA)	776 ± 33.8	1850 ± 183	22090 ± 6190	n.d.	156
	1 (+DNA)	786 ± 4.83	1740 ± 80.7	26620 ± 7620	0.45 ± 0.18	175
	1 (+DNA, purified)	797 ± 0.19	1500 ± 10.5	9400 ± 6150	n.d.	151
	2	728 ± 12.2	4090 ± 118	18630 ± 4870	n.d.	257
	3	713 ± 0.63	8200 ± 581	22120 ± 9640	n.d.	120
	4	698 ± 1.09	13900 ± 483	32180 ± 8820	n.d.	129
Ncd						
	1 (+DNA)	−100 ± 14.0	*−270 ± 27.4	7220 ± 7200	2.2 ± 0.35	133
	1 (+DNA, purified)	−101 ± 16.1	*−318 ± 65.0	5770 ± 2390	n.d.	86
	2	−150 ± 12.0	−1330 ± 208	10340 ± 3650	1.2 ± 0.22	128
	3	−146 ± 6.95	−3360 ± 462	10960 ± 3750	0.76 ± 0.10	203
	4	−163 ± 9.37	−6080 ± 979	14290 ± 1690	0.59 ± 0.09	173

Velocities and run lengths were determined from the arithmetic mean. The minus (−) symbol refers to the polarity of the MT. Errors for velocities and run lengths are given as the standard error of means. Errors for MT lengths are given as the standard deviation of all MTs used. n is the total number of runs that were scored for each construct from three independent experiments. *Note that the scored run length for single Ncds is an overestimation. n.d., not determined.

Table S2. Effects of the Arrangement of Two Coupled Kinesin-1 Motors

Linker Type	Spacing (nm)	Velocity (nm s^{-1})	Run Length (nm)	MT Length (nm)	n
Flexible					
	1.1	651 ± 20.0	2830 ± 86.3	11600 ± 7530	549
	4.2	615 ± 15.0	2540 ± 635	14250 ± 7030	277
	7.6	719 ± 5.8	2850 ± 57.0	12310 ± 7210	300
	18.3	673 ± 11.6	3290 ± 382	11520 ± 7780	411
	22.7	728 ± 12.2	4090 ± 118	18630 ± 3940	257
	44.6	730 ± 42.7	4170 ± 531	14630 ± 5610	150
	64.2	765 ± 11.1	4440 ± 55.0	14890 ± 4530	151
Semi-flexible					
	19.7	613 ± 24.4	4460 ± 350	14840 ± 6640	231
	39.4	719 ± 28.1	4270 ± 197	15760 ± 4020	230
	58.8	704 ± 25.1	5030 ± 525	13300 ± 6080	233
Rigid					
	0.68	603 ± 49.0	4690 ± 826	12940 ± 5840	400
	3.0	527 ± 68.0	4780 ± 323	14280 ± 7010	273
	7.0	606 ± 37.2	4840 ± 645	17130 ± 8120	395
	17.0	568 ± 5.3	4180 ± 436	10750 ± 6320	235
	19.7	670 ± 26.0	3870 ± 396	12920 ± 4150	209
	37.0	681 ± 30.8	3800 ± 303	13460 ± 5300	200
	52.1	736 ± 12.9	4560 ± 714	14720 ± 5710	200

Velocities and run lengths were determined from the arithmetic mean. Spacing is given as the end-to-end length of DNA oligomer. Errors for velocities and run lengths are given as the standard error of means. Errors for MT lengths are given as the standard deviation of all MTs used. n is the total number of runs that were scored for each construct from three independent experiments.

Table S3. Effects of the Arrangement of Two Coupled Ncd Motors

Linker Type	Spacing (nm)	Velocity (nm s^{-1})	Run Length (nm)	MT Length (nm)	n
Flexible					
	1.1	−189 ± 2.4	−2800 ± 610	11700 ± 6460	195
	7.6	−196 ± 13.3	−1760 ± 78.1	8650 ± 4530	155
	18.3	−192 ± 6.0	−1520 ± 126	10370 ± 5700	205
	22.7	−150 ± 12.0	−1330 ± 208	10340 ± 6130	128
	44.6	−177 ± 10.4	−1500 ± 250	16530 ± 6730	157
	58.8	−188 ± 1.7	−1400 ± 46.5	16370 ± 5590	220
Rigid					
	0.68	−145 ± 31.5	−3240 ± 36.5	12770 ± 6220	181
	7.0	−173 ± 11.3	−2630 ± 97.7	14110 ± 6030	179
	17.0	−159 ± 34.2	−1660 ± 27.2	12740 ± 3610	217
	19.7	−164 ± 8.5	−1440 ± 295	19680 ± 9460	164
	37.0	−185 ± 4.4	−1660 ± 112	14670 ± 9570	319
	52.1	−162 ± 8.1	−1480 ± 56.4	16800 ± 9780	187

Velocities and run lengths were determined from the arithmetic mean. Spacing is given as the end-to-end length of DNA oligomer. Errors for velocities and run lengths are given as the standard error of means. Errors for MT lengths are given as the standard deviation of all MTs used. n is the total number of runs that were scored for each construct from three independent experiments.

Table S4. Collective Force Production by Kinesin-1 and Ncd

Motor Protein	Number of Motors	Spacing (nm)	Maximum Force (pN)	n
Kinesin-1				
	1	n.a.	5.2 ± 0.1	244
	2	7.0	5.8 ± 0.1	556
	3	6.0	6.3 ± 1.1	340
	4	6.0	6.7 ± 0.1	555
	2	22.7	6.5 ± 0.8	184
	3	22.7	6.7 ± 1.6	82
	4	22.1	8.0 ± 0.5	614
Ncd				
	2	7.0	0.56 ± 0.14	306
	3	6.0	1.01 ± 0.32	280
	4	6.0	1.56 ± 0.17	342
	2	22.7	0.71 ± 0.02	360
	3	22.7	1.00 ± 0.10	178
	4	22.1	1.40 ± 0.07	290

Spacing is given as the end-to-end length of DNA oligomer. Maximum forces were determined from the arithmetic mean. Errors for maximum forces are given as the standard error of means. n is the total number of runs that were scored for each construct from three independent experiments. n.a., not applicable.

Table S5. Tug-of-war between Single Kinesin-1 and Several Ncds

Number of Motors	Velocity (nm s^{-1})	Run Length (nm)	Binding Time (s)	MT Length (nm)	n
1 kinesin-1 + 1 Ncd	283 ± 47.2	2800 ± 410	12.5 ± 3.09	22100 ± 4470	224
1 kinesin-1 + 2 Ncds	246 ± 21.1	2560 ± 491	14.7 ± 3.44	16010 ± 4540	203
1 kinesin-1 + 3 Ncds	158 ± 16.0	3330 ± 656	27.0 ± 6.54	17120 ± 3880	209
1 kinesin-1 + 4 Ncds	175 ± 69.2	4360 ± 1120	36.1 ± 1.90	18880 ± 3180	194

Velocities and run lengths were determined from the arithmetic mean. Errors for velocities and run lengths are given as the standard error of means. Errors for MT lengths are given as the standard deviation of all MTs used. n is the total number of runs that were scored for each construct from three to four independent experiments.

Table S6. Examples of Fitted Parameter Sets for Motility Assays at Low Load

Parameter	Kinesin-1	Ncd
Stepping rate (k_{step}, s^{-1})	98.3	22.0
Linker stiffness (k, pN nm^{-1})	*0.2	0.2
On-rate (π_0, s^{-1})	*7.0	*7.0
Off-rate (ε_0, s^{-1})	0.4	0.45
Critical detachment force (forward, $F_{d,F}$, pN)	3.0	*1.8
Scale factor for critical detachment force (backward/forward)	1.0	1.3
Stall force (F_s, pN)	6.8	0.2
Force–velocity relationship (w)	2.0	1.0
Diffusion coefficient ($\times 10^{-3}$ μm^2 s^{-1})	–	2.0
Lower limit of random steps (nm)	–	*0.25

*Free parameters used for parameter scanning.

Table S7. Examples of Fitted Parameter Sets for Optical Trapping Assays

Parameter	Kinesin-1 (1)	Kinesin-1 (2)	Ncd (1)	Ncd (2)
Stepping rate (k_{step}, s^{-1})	98.3	98.3	22.0	22.0
Linker stiffness (k, pN nm^{-1})	0.25	0.25	0.25	0.25
On-rate (π_0, s^{-1})	*0.51	*0.6	*10.8	*9.7
Off-rate (ε_0, s^{-1})	*0.75	*0.4	*4.3	*3.6
Critical detachment force (forward, $F_{d,F}$; pN)	*6.6	*3.6	*4.2	*2.3
Scale factor for critical detachment force (backward/forward)	1.0	1.0	1.3	1.3
Stall force (F_s, pN)	6.8	6.8	0.2	0.2
Force–velocity relationship (w)	2.0	2.0	1.0	1.0

*Free parameters used for parameter scanning.